Published in Neuroscience 87, issue 4, 741-766, 1998
which should be used for any reference to this work

THE SPIKE TRAINS OF INHIBITED PACEMAKER NEURONS SEEN THROUGH THE MAGNIFYING GLASS OF NONLINEAR ANALYSES

J. P. SEGUNDO,*†|| G. SUGIHARA,‡ P. DIXON,‡ M. STIBER§ and L. F. BERSIER‡¶

*Department of Neurobiology, University of California, Los Angeles, CA 90095-1763, U.S.A.

†Facultad de Ciencias, Universidad de la República, 11200 Montevideo, Uruguay

‡Scripps Institute of Oceanography, University of California, San Diego, La Jolla, CA 92093-0202, U.S.A.

§Computing and Software Systems, University of Washington, Bothell, WA 98081-4900, U.S.A.

¶Biological Institute, Pérolles, CH-1700, Switzerland

Abstract—This communication describes the new information that may be obtained by applying nonlinear analytical techniques to neurobiological time-series. Specifically, we consider the sequence of interspike intervals T_i (the ''timing'') of trains recorded from synaptically inhibited crayfish pacemaker neurons. As reported earlier, different postsynaptic spike train forms (sets of timings with shared properties) are generated by varying the average rate and/or pattern (implying interval dispersions and sequences) of presynaptic spike trains. When the presynaptic train is Poisson (independent exponentially distributed intervals), the form is ''Poisson-driven'' (unperturbed and lengthened intervals succeed each other irregularly). When presynaptic trains are pacemaker (intervals practically equal), forms are either ''*p:q* locked'' (intervals repeat periodically), ''intermittent'' (mostly almost locked but disrupted irregularly), ''phase walk throughs'' (intermittencies with briefer regular portions), or ''messy'' (difficult to predict or describe succinctly). Messy trains are either ''erratic'' (some intervals natural and others lengthened irregularly) or ''stammerings'' (intervals are integral multiples of presynaptic intervals).

The individual spike train forms were analysed using attractor reconstruction methods based on the lagged coordinates provided by successive intervals from the time-series T_i. Numerous models were evaluated in terms of their predictive performance by a trial-and-error procedure: the most successful model was taken as best reflecting the true nature of the system's attractor. Each form was characterized in terms of its dimensionality, nonlinearity and predictability.

(1) The dimensionality of the underlying dynamical attractor was estimated by the minimum number of variables (coordinates T_i) required to model acceptably the system's dynamics, i.e. by the system's degrees of freedom. Each model tested was based on a different number of T_i; the smallest number whose predictions were judged successful provided the best integer approximation of the attractor's true dimension (not necessarily an integer). Dimensionalities from three to five provided acceptable fits.

(2) The degree of nonlinearity was estimated by: (i) comparing the correlations between experimental results and data from linear and nonlinear models, and (ii) tuning model nonlinearity via a distance-weighting function and identifying the either local or global neighborhood size. Lockings were compatible with linear models and stammerings were marginal; nonlinear models were best for Poisson-driven, intermittent and erratic forms.

(3) Finally, prediction accuracy was plotted against increasingly long sequences of intervals forecast: the accuracies for Poisson-driven, locked and stammering forms were invariant, revealing irregularities due to uncorrelated noise, but those of intermittent and messy erratic forms decayed rapidly, indicating an underlying deterministic process.

The excellent reconstructions possible for messy erratic and for some intermittent forms are especially significant because of their relatively low dimensionality (around 4), high degree of nonlinearity and prediction decay with time. This is characteristic of chaotic systems, and provides evidence that nonlinear

||To whom correspondence should be addressed at the University of California.

Abbreviations: *b*, neighborhood size; BVP, Bonhoeffer–van der Pol model; CV, coefficient of variation; Δt, time-step; *E*, embedding dimension; HH, Hodgkin–Huxley model; *i*, order (1, 2,...) of postsynaptic spike and interval; *I*, average presynaptic interval; IF, inhibitory fiber; I_k, *k*th presynaptic interval; IPSP, inhibitory postsynaptic potential; *j*D, with *j* dimensions; *k*, order (1, 2,...) of presynaptic spike and interval; *p*, *q*, *r*, integers (1, 2,...); PSP, postsynaptic potential; PTC, phase transition curve; ρ, correlation coefficient; SAO, slowly adapting stretch receptor organ or postsynaptic neuron; s_k, time when the *k*th presynaptic spike occurs; *t*, *z*, statistics; *T*, average postsynaptic interval; t_i, time when the *i*th postsynaptic spike occurs; T_i, *i*th postsynaptic interval; T_P, prediction time; θ, nonlinearity coefficient in model.

couplings between relatively few variables are the major source of the apparent complexity seen in these cases.

This demonstration of different dimensions, degrees of nonlinearity and predictabilities provides rigorous support for the categorization of different synaptically driven discharge forms proposed earlier on the basis of more heuristic criteria. This has significant implications. (1) It demonstrates that heterogeneous postsynaptic forms can indeed be induced by manipulating a few presynaptic variables. (2) Each presynaptic timing induces a form with characteristic dimensionality, thus breaking up the preparation into subsystems such that the physical variables in each operate as one formal parameter or degree of freedom. A system's partitions differ because of component subsystems and/or dynamics: the set of all partitions is probably large and continuous. Driver-induced partitions have general theoretical interest, and provide guidelines for identifying the responsible physical variables. (3) Because forms tolerate changing conditions and are encountered widely (e.g., along transients), it is hypothesized that they are elementary building blocks for many synaptic codings. Codings are linear if postsynaptic forms have the same spectral components as the presynaptic pacemaker, or nonlinear if novel components arise as with, respectively, 1:1 locked or erratic trains. This is relevant to network operations where regularity and irregularity are often vital. (4) Rigorously identifying spike train forms in experimental data from living preparations allowed matchings with available theoretical computations and considerations. Relevant models are based either on iterations of maps derived from rhythm resettings by isolated arrivals or on Bonhoeffer–van der Pol formulations: such models generate, respectively, only periodic locking and phase walk throughs, or all forms. This precise and broad conceptual context explains and predicts outcomes, recognizes data/theory discrepancies, and identifies their reasons (e.g., after-effects, noise). (5) Accordingly, forms pertain to universal behavior categories called ''noisy'', ''periodic'', ''intermittent'', ''quasiperiodic'' or ''chaotic'' whose available theories provide valuable contexts for genuinely physiological issues. Thus, experimental design and thinking benefit from significant insights about the dynamics of pacemaker-driven pacemakers, the simplest of all synaptic codings.

Key words: pacemaker, stretch receptor, dynamics, nonlinearity, chaos, noise.

CONTENTS

1. INTRODUCTION

This communication is concerned with the regular and irregular spike trains of living, synaptically driven pacemaker neurons. ''Pacemaker neurons'' spontaneously generate regular spike trains, also called ''pacemaker'', whose interspike intervals are close to their average. Early work had recognized that pacemakers could be irregularized by presynaptic arrivals, either irregular or, more surprisingly, regular.[29,42,48,53]

Recent publications inspired by Dynamical Systems Theory led experimental neuroscientists to examine issues more fundamental than those addressed by preparation-specific models.[1,2,8,10,12–14,19,24–27,31–34,36,40,43,44,51,52,54,58,72,73] This included identification of spike trains whose timings were assigned to universal categories of system behavior (periodic, nearly periodic or intermittent, deterministically unpredictable or chaotic, stochastically unpredictable or noisy). The ''timing'' is composed of the instants when spikes occur (see below).

A variety of preparations and neurons driven by periodic currents have been used. Observations often concentrated on the evolution of the membrane potential $V(t)$, plots of $V(t)$ versus $V(t + \Delta t)$, and plots of $V(t)$ versus $\mathrm{d}V(t)/t$. Hayashi and Ishizuka, for example, studied epileptic hippocampal slices, and provided evidence for synchronous periodic and chaotic activities.[25] A few observations concentrated

on the spike trains themselves. Hayashi and collaborators diagnosed both intermittency and chaos, based on the structure of point clusters on interval return maps (plots of each interspike interval versus a subsequent one).[26] Rapp *et al*. suggested that irregular spike trains that met certain quantitative criteria might be chaotic.[44] Mpitsos *et al*., observing maps of rates or intervals, found that neighboring points flowed together more often than remote ones and that trajectories separated and reordered quickly: this suggested attractor stretchings and foldings consistent with chaos.[34] Takahashi and collaborators' analysis supported their claim that spike trains were periodic, intermittent or chaotic.[68] Diez Martínez *et al*. found that periodic sensory stimulation, depending on the rate of the stimulus, resulted in interval return maps compatible with periodic and intermittent forms separated by tangent bifurcations.[10]

Particularly relevant here are experiments with controlled synaptic driving of living neurons. We know of only two. In *Onchidium* neurons, Hayashi diagnosed ''1:1 entrained'' trains when interspike intervals were all equal and potential $V(t)$ return maps had a single tight cluster on the diagonal, and chaos when intervals were heterogeneous and maps not invertible.[24] In inhibitory synapses, Segundo *et al*. used return maps, recurrence plots and spectra to classify trains driven by pacemaker patterns into forms called lockings, intermittencies, phase walk throughs, messy erratic and messy stammerings.[51,52] A train's ''pattern'' reflects interval dispersion and sequence, irrespective of their averages; a ''form'' is a class of timings with specified properties. These publications contributed to understanding spike trains in many living, synaptically driven neurons, as did the concepts and predictions provided by their proposed models. Pacemaker-driven trains and forms, plus those driven by Poisson patterns, form the background of the present effort. A ''Poisson'' pattern has exponentially distributed, serially independent intervals greater than a minimum ''dead-time''. Earlier analyses have limitations, however. Indeed, after critically evaluating such work, Glass stresses that, whereas their conclusions are straightforward and convincing when targeting deterministic equations, they demand extreme caution when dealing with experimental time-series.[14] Accordingly, then, further work is necessary. Firstly, rationales for form identification and classification have been either indirect and only via perceived compatibilities with model-generated templates or, if direct and via data, have reflected essentially qualitative evaluations. Secondly, form interpretation has ignored the issues of dimensionality, nonlinearity and irregularity. These mesh intimately with the nonlinear theory underlying spike trains and their physiological considerations; clarification of these issues is conceptually and practically important.[63] The present analysis of synaptically driven pacemaker neurons uses exclusively experimental data from living crayfish preparations to reassess form identification and tackle those issues. The endeavor, neither conceptually nor technically trivial, is facilitated by approaches of recent vintage suited for physiology where systems are often not understood thoroughly and data sets are restricted: their suitability has been proven in disparate fields.[23,63–67]

Efforts parallel to those reported here target similar objectives. Xie *et al*. analysed ''unstimulated'' trains from rat brains and showed uniform predictability and thus a noisy genesis in their data, though not necessarily everywhere.[73] Longtin and collaborators have contributed significantly by way of analysing spike trains in auditory and somatosensory systems where some nonlinearity was detected[31] of theoretical considerations on the possibility of reconstructing attractors on the basis of intervals between events,[43] and finally of comparisons of alternative models of trains along cold receptor afferents.[32] Chillemi *et al*. demonstrated chaotic behavior in snail neurons driven by sinusoidal currents.[8] Moss forced crayfish receptors and diagnosed chaos after analysing statistically rare events in the interval sequence.[33]

An indispensable and well-tested scientific strategy involves matching the restricted data sets from living preparations with exhaustive and precise dissections allowed by formal models. This strategy, as applied to periodically driven oscillators (see Discussion), has been based on either iteration of one-dimensional maps, on, say, leaky integrators or Bonhoeffer–van der Pol models (BVPs), or on those incorporating physical variables. Glass and collaborators introduced the strategy and successfully implemented it using heart cell aggregates.[14,16–19,21,22,41] Similar steps have been followed with periodically inhibited slowly adapting stretch receptor organ or postsynaptic neurons (SAOs).[29,30,42,48,49,60,70] The data-based classification of experimentally generated spike train forms attempted here confers rigor to this endeavor, and thus can contribute significantly.

2. EXPERIMENTAL PROCEDURES

The trains analysed here (see below) came from a data set of earlier publications that included 245 pairs of corresponding trains obtained from 26 slowly adapting stretch receptor organs (SAO) of crayfish *Procambarus clarkii*.[29,51,52,55] Section 2.1. summarizes the basic experimental and statistical methodologies whose full details are in the earlier papers.[29,51,52,54,56,58,59] Section 2.2. identifies the subset of that broader data set dealt with here and describes the more specialized procedures used for their analyses.

2.1 *Data generation*[51,59]

In the SAO, the presynaptic inhibitory fiber (IF) releases GABA; the postsynaptic receptors resemble vertebrate type A, affecting chloride conductances. Conventional procedures were utilized for preparation dissection and maintenance in van Harreveld's saline around 14°C, for simultaneous electrical recording of presynaptic and

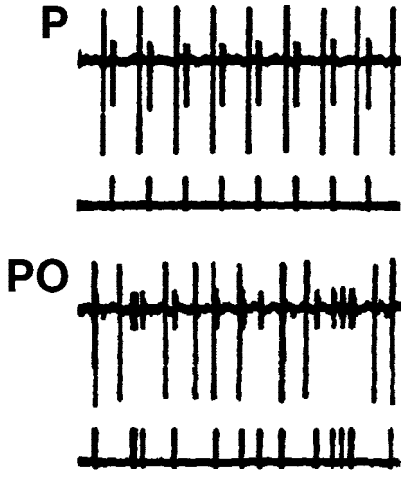

Fig. 1. Spike trains. Locking (P): presynaptic pacemaker, i.e. periodic, train at close to the postsynaptic natural average. Poisson-driven (PO): presynaptic Poisson train at intermediate average. Traces are voltages recorded extracelluarly along ongoing time: upper, presynaptic train (small spikes) and postsynaptic train (large spikes); lower, stimulus pulses delivered to the inhibitory fiber. The timescale is given by sweep durations of approximately 1.000 s. Adapted from Fig. 13 in Segundo *et al.*[57]

postsynaptic voltages with a single electrode, and for electrical presynaptic stimulation with another. Recordings are illustrated by the upper traces of each portion in Fig. 1; the lower traces illustrate the stimulating pulses.

Controlled trains of electrical pulses with selected rates and patterns delivered to the IF triggered presynaptic spike trains. Each pulse triggered a single presynaptic spike and the presynaptic train was identical to the pulse train (except for a minor delay as IF spikes followed triggering pulses by practically 5 ms): hence, both had the same form, i.e. class of timings with specified properties. The electrical activities of the synaptically connected neurons, as well as the stimulating pulses, were stored on magnetic tape; all processing was performed on these recordings (Fig. 1). The spikes from the IF, the SAO and, when also triggered by the pulses, the neighboring fast receptor neuron were in one trace (Fig. 1, upper trace). Spike separation was achieved by passing this record through a conventional window circuit because spike amplitudes scaled roughly like, respectively, 1, 6 and 10 (and all exceeded the background noise by far). Spike separation was followed spike by spike using a multi-channel oscilloscope and thus checked for being correct. Cases where separation was uncertain were rare and, in both the earlier and present papers, excluded from the data set.

Figure 1 displays original recordings that allow a visual impression of the raw data. As noted above, the upper trace shows both the presynaptic and postsynaptic trains of, respectively, small and large spikes (the fast adapting neuron was not triggered). The regular pacemaker-driven locked form labelled P and the irregular Poisson-driven form PO are described in Results together with the other forms.

Presynaptic spike trains were controlled. Rates were from 0.4 to 1.5 times the natural rate (Table 3). All patterns included serially independent interspike intervals, and were either highly irregular Poisson or highly regular pacemaker. ''Poisson'' patterns approximated theoretical Poisson processes: intervals I_k had a minimum value (reflecting refractoriness), almost exponential densities and large dispersions (coefficient of variation, $CV \approx 0.64$) around their average I. Pacemaker patterns approximated theoretical clocks, the I_k dispersing minimally ($CV \approx 0.0001$) around I.

The times of occurrence of individual spikes—s_k for the kth inhibitory spike, t_i for the ith postsynaptic spike (k, $i = 1, 2,...$)—were identified and stored using specialized hardware and software. Errors when measuring these times were not above 0.25 ms (and judged negligible, see below). s_k and t_i constitute the train's timing (see above), described also and equivalently by the time series of presynaptic intervals (I_k), postsynaptic intervals (T_i) and phases. ''Phases'' are cross-intervals from a postsynaptic to the most recent presynaptic spike, implying the driven event's position relative to the driver's sequence.[51,52,56,58,59] ''Phase'' in, say,[16,17,20–22,29,36,37,42] means the driver event's position relative to the spontaneous cycle of the driven oscillator.

Postsynaptic time-series are plotted as ''basic graphs'' (Fig. 2). To each spike corresponds a point (t_i,T_i) whose abscissa is its time of occurrence and whose ordinate is the preceding postsynaptic interval. They thus tell us what the individual intervals are, and how they evolve along time in the individual train. Point distributions can be more or less dispersed or clustered. ''Cluster'', as used here (and for return maps, see below), refers to a set of many points grouped together in close proximity with many others, and therefore presenting a high density: i.e. to a set with many points in a region restricted in one or more dimensions. Clusters so defined may have any shape: those described below concentrate around zero-dimensional centers, one-dimensional lines or two-dimensional planar figures. The computer-controlled drawing of each basic graph was slowed down allowing its build-up along time to be followed point by point: because of this, it was possible to both discern the details and extract a valuable overview of how the spike train evolves along time and sequence.

Stationary portions (segments of which are in Fig. 2) were identified in each spike train and, within each, conventional point process statistics were estimated (see Tables 1–3). Average rates over the entire stationary portion (called ''rates'' here) reflect the overall intensity of spike generation, as do the average intervals; under present conditions, the respective estimates are reciprocals.[58] Statistics evaluating interval dispersions or orderings reflect the generation's fluctuations, implying the train's pattern, for which ''pacemaker'', ''Poisson'', ''bursty'', etc., are traditional designations. The functional significance of both averages and patterns in general is an unavoidable consequence of the undisputed fact that dissimilar timings are associated with dissimilar functional states;[56,58,59] the meaningful experimental question to be asked is the domain in which they are significant in particular cases. Dispersions were evaluated by interval standard deviations, coefficients of variation and histograms, and sequences by the second-order statistics quantifying correlations between portions separated along time or order. Second-order statistics are the continuous autointensity function (estimated by the autocorrelation histogram) whose argument is time t and the discrete autocorrelation sequence of correlation coefficients whose argument is serial order i; the corresponding continuous spectra are expressed as, respectively, cycles/s (Hz) or cycles/order. By the magnitudes, locations and separations of their peaks and troughs, these statistics evaluate whether trains are regular and predictable, irregular and unpredictable, or in between. Patterns—i.e. dispersions and sequences—provided the critical criteria upon which forms were classified initially, and separated the forms into pacemaker-driven locked, intermittent, phase walk throughs, messy erratic, messy stammering and Poisson-driven.[51,52] The earlier papers include the full description of those statistics, as well as how the spike train patterns led to separation of spike trains into locked, intermittent, phase walk through, messy erratic, messy stammering or Poisson-driven forms (see also Results and Discussion).[29,51,52] The individual forms are analysed further and more rigorously in the present communication: this is described in the next subsection.

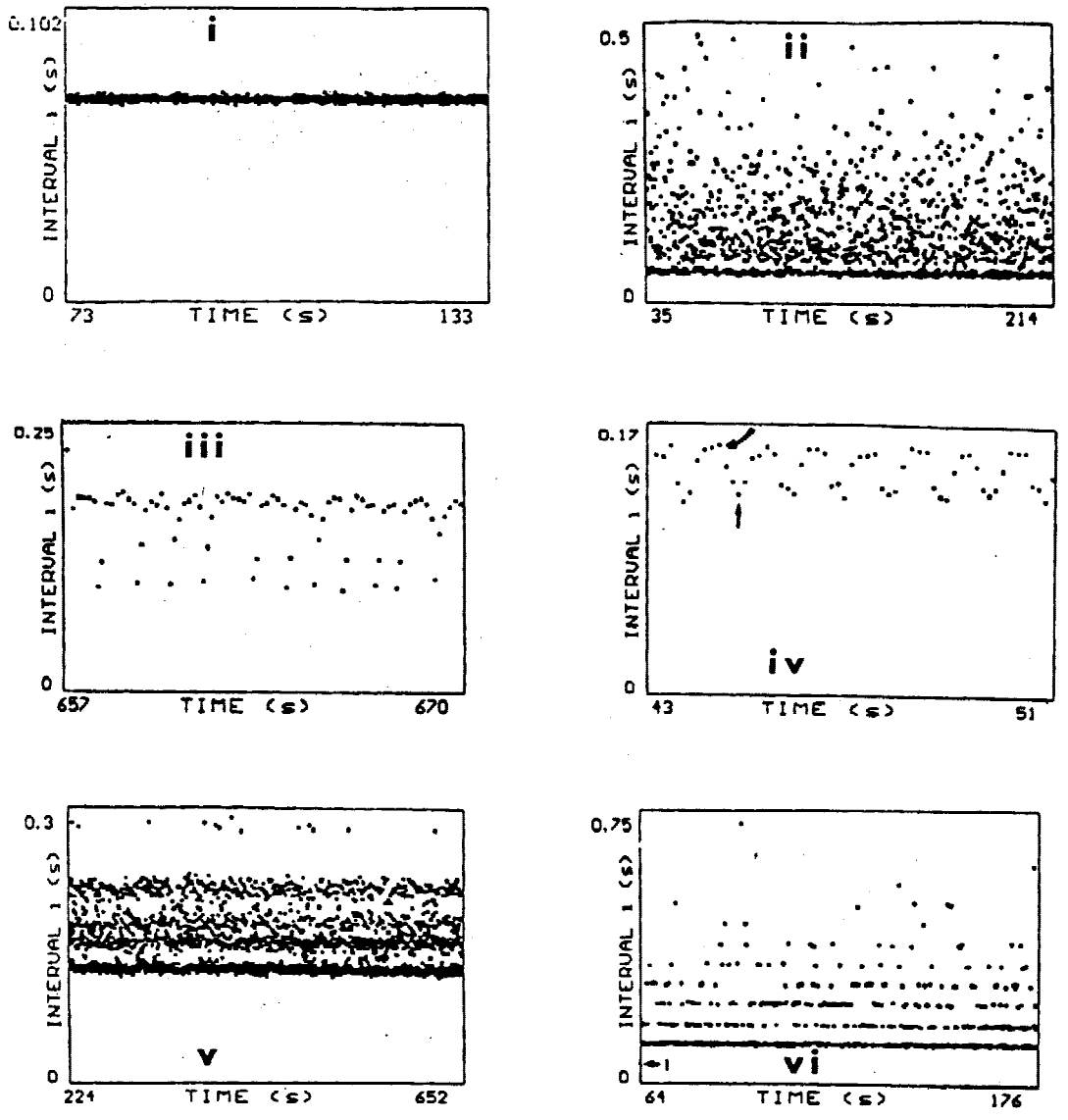

Fig. 2. Basic graphs. Each point corresponds to a spike in a segment of the stationary portion of the postsynaptic spike train whose timing is described by the time-series of its interspike intervals. Abscissa, time t_i of ith spike occurrence; ordinate, preceding interval T_i. Panels correspond to pacemaker drivings at different averages (intervals, rates) in i, iii–vi, and to a Poisson driving in ii. Their statistics are in Table 2; the corresponding natural postsynaptic and presynaptic ones are in Tables 1 and 3. (i) 1:1 locking: points in a vertically tight horizontally extended cluster whose ordinate is the presynaptic interval *I*. Panel i is from a neuron with a natural rate of 19.14 s^{-1} pacemaker-driven at 14.00 s^{-1} (normalized ratio 0.73); the resulting postsynaptic rate was 14.00 s^{-1}. Same form but not same trains, as in Fig. 3 and Plate B in Ref. 51 and Figs 3 (later epochs), 5 and 9 in Ref. 52. (ii) Poisson-driven: points in a dense horizontal cluster or dispersed above, and a sparse band in between: these reflect, respectively, natural intervals without arrivals, intervals lengthened irregularly by arrivals, and that lengthenings had a minimum. Panel ii is from a neuron with natural rate 15.3 s^{-1} Poisson-driven at 16.00 s^{-1} (normalized 1.05); the resulting postsynaptic rate was 8.58 s^{-1}. Same form and train as in Fig. 2 in Ref. 55. (iii) Intermittent: a predominant regular, almost 1:1 locked portion is interrupted occasionally, briefly and irregularly. Panel iii is from a case where a neuron with a natural rate of 6.73 s^{-1} was driven at a rate of 5.52 s^{-1} (ratio 0.82); the resulting postsynaptic rate was 6.21 s^{-1}. Same form, but not the same trains as in Fig. 5 (later epoch) and Plate C in Ref. 51 and Figs 3 (first epoch), 4B,E and 7 (late epoch) in Ref. 52. (iv) Phase walk through. In this special intermittent train, almost horizontal clusters (curved arrow) or more vertical clusters (vertical arrow) represent the regularly firing portion or the irregular bursts, respectively. Phase walk throughs are special intermittent trains where the regular portions are relatively less prevalent (and the phases—not shown—evolve in special standardized ways). Panel iv is from a case where a neuron with a natural rate of 8.5 s^{-1} was driven at a rate of 6.14 s^{-1} (ratio 0.72); the resulting postsynaptic rate was 7.13 s^{-1}. Adapted from, and including the same train as Fig. 6 and Plate D in Ref. 51. (v) Messy erratic: several clusters separated by not altogether empty sparse bands indicate that intervals though exhibiting moderate preference for certain values, have substantial dispersions: the shortest intervals close to *N* lack arrivals. Panel v is from a case where a neuron with a natural rate of 7.84 s^{-1} was driven at a rate of 3.77 s^{-1} (ratio 0.48); the resulting postsynaptic rate was 6.54 s^{-1}. Same form, but not the same trains as in Figs 8, 11 (some epochs) and Plate E of Ref. 51. (vi) Messy stammerings: intervals are multiples of the presynaptic interval I (arrow). Panel vi is from a case where a neuron with a natural rate of 14.4 s^{-1} was driven at a rate of 18.2 s^{-1} (ratio 1.26); the resulting postsynaptic rate was 6.41 s^{-1}. Adapted from, and including the same train as Fig. 9 and Plate F in Ref. 51.

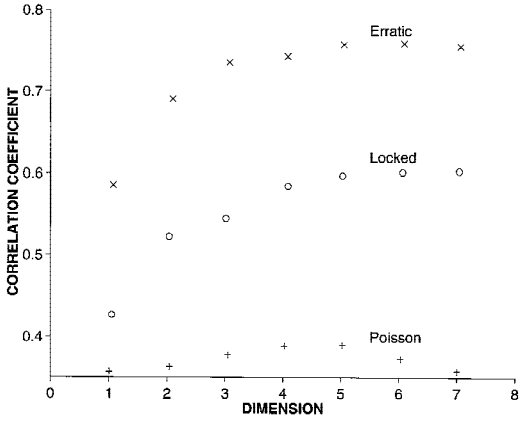

Fig. 3. Embedding dimension, correlation coefficients and form (see Table 4). Dimension versus correlation coefficient ρ (at the neighborhood where it is highest). Open circles, 1:1 locked: coefficients increase with dimension, becoming acceptable at four or five. Neuron with a natural rate of 19.14 s^{-1} pacemaker-driven at 14.00 s^{-1} (normalized ratio 0.73); the resulting postsynaptic rate was 14.00 s^{-1}. Same form but not same trains, as in Fig. 3 and Plate B in Ref. 51 and Figs 3 (later epochs), 5 and 9 in Ref. 52. Pluses, Poisson-driven: coefficients increase little with dimension, peak at four, and then decrease. Neuron with natural rate 15.3 s^{-1} Poisson-driven at 16.00 s^{-1} (normalized 1.05); the resulting postsynaptic rate was 8.58 s^{-1}. Same form and train as in Fig. 2 in Ref. 55. Crosses, erratic: coefficients increase with dimension, becoming acceptable at four or five. Neuron with natural rate 7.84 s^{-1} pacemaker-driven at 3.77 s^{-1} (ratio 0.48); resulting postsynaptic rate was 6.54 s^{-1}. Same form as in Figs 8, 11 (some epochs) and Plate E of Ref. 51, but not the same trains. The same plots for intermittencies (not depicted) either resemble locked or erratic ones, or are in between; data for phase walk throughs were not plotted because stationary samples were not large enough to justify conclusions. Additional statistics are in Tables 1–3.

Table 1. Natural postsynaptic statistics. Taken from the stationary postsynaptic spike train immediately preceding the form indicated in the left column: (i) locked or periodic, (ii) Poisson-driven, (iii) intermittent, (iv) phase walk through, (v) messy erratic, (vi) messy stammering

Form	Sample size	Average interval μ (s)	Standard deviation σ (s)	CV	Average rate (s^{-1})
i	388	0.052	0.0006	0.012	19.14
ii	153	0.065	0.0012	0.018	15.3
iii	68	0.149	0.003	0.021	6.73
iv	254	0.118	0.003	0.024	8.5
v	325	0.128	0.008	0.062	7.84
vi	559	0.069	0.0002	0.020	14.4

2.2 *Nonlinear time-series methods* [23,63,67]

Specialized methods, time and effort consuming, were only applied to a subset of the data from the earlier papers:[29,51,52,55] each train in this subset was typical of a particular form, i.e. exhibited unmistakably all the features required by the diagnostic criteria proposed by Segundo *et al.*;[51] the subset spanned all form categories and included up to three of each. Accordingly, the present analyses can lead legitimately to asserting that a train with a particular form can exhibit a particular combination of dimensionality, nonlinearity and predictability into the future. However, because of the relatively small number of trains so dissected, analyses cannot lead to reliable estimates of the proportion of trains with a particular form that exhibit those features.

Table 2. Driven postsynaptic statistics. Taken from the stationary postsynaptic trains where forms were analysed. The stationary portions of phase walk throughs were too short for reliable estimates, and omitted

Form	Sample size	Average interval μ (s)	Standard deviation σ (s)	CV	Average rate (s^{-1})
i	1255	0.071	0.0009	0.013	14.00
ii	1451	0.117	0.075	0.64	8.58
iii	920	0.161	0.030	0.186	6.21
iv	142	0.140	0.012	0.086	7.13
v	2784	0.153	0.032	0.210	6.54
vi	735	0.156	0.082	0.526	6.41

Typical cases illustrate pacemaker-driven forms in all figures of the earlier and the present papers: the individual panels are extracted either from the same trains (though different epochs may be included) for phase walk throughs and stammerings, or from different trains for lockings, intermittent and erratic forms. Less typical, borderline cases were excluded. Indeed, it has been noted (and is discussed below) that diagnostic criteria are either qualitative or, if quantitative, require margins of tolerance when applied; forms therefore do not separate cuttingly, and borderline, difficult-to-categorize trains exist.

Two sources of variation in natural time-series are measurement or observational error and dynamic complexity. While measurement error has hindered the successful application of the techniques described herein to other fields within the biological sciences,[63] it was minimal here (see above), making this system a good candidate for such studies. Indeed, errors under 0.25 ms (see above), if compared to the intervals of tens or hundreds of milliseconds were well below 2%.

We shall now develop the intuitive notions behind these methods; further technical expositions are available elsewhere.[6,14,19,47,63,66,67] In the absence of observational error, the dynamic complexity of a system may be thought of as the product of the number of interacting variables—the system's degrees of freedom—and the degree of nonlinearity in the couplings between those variables (e.g., see Ref. 63). Because predictability is an important goal of any time-series modeling effort, dynamic complexity is often subcategorized into components alluded to as ''signal'' which may be modeled and forecast acceptably, and as ''process noise'', which arises from system dynamics that are not explicitly modeled. Process noise is the apparent stochasticity that comes from ignorance of the full system dynamics. Thus, it is important to recognize that this classification, idiosyncratic to the study at hand, reflects the cut-off point of our understanding, rather than a separation of fundamental ''types'' of interactions. In other words, variability that cannot be accounted for by observational error must have a dynamical origin, though our efforts to describe the responsible dynamics inevitably fall short of fully understanding them. Therefore, this subdivision of dynamic complexity into signal and process noise is an artificial construct, and is really a description of the point at which human understanding ends and ignorance begins (see Refs 14, 63).

Fundamental to dynamical systems theory are certain concepts that are explained in easily available references to which the reader is referred.[4,19,23,38] In summary, a system is composed of dynamically coupled ''state variables'', and at each instant represented by a point in the ''state space'' whose axes are those variables. The number of these

Table 3. Presynaptic statistics. The average inhibitory rate is normalized by expressing it as its ratio relative to the postsynaptic natural average rate

Form	Average sample size	Standard interval μ (s)	Deviation σ (s)	CV	Average rate (s^{-1})	Normalized
i	823	0.071	7.10^{-5}	0.001	14.00	0.73
ii	2865	0.062	0.047	0.758	16.00	1.05
iii	706	0.181	0.00008	0.0004	5.52	0.82
iv	31	0.163	0.00005	0.0003	6.14	0.72
v	5024	0.265	0.0003	0.001	3.77	0.48
vi	2364	0.055	0.0002	0.004	18.2	1.26

variables is the space's ''dimension''. As time passes, the state point moves along a ''trajectory'': in so-called ''dissipative systems'', trajectories approach and stay on an ''attractor'', a subset of the space to which the system returns if perturbed.[66] Attractors are closed limit cycles for periodic behaviors, entire toroidal (doughnut-shaped) surfaces covered densely by never closing trajectories for quasiperiodicities, or stretched, folded and ''strange'' for chaotic trajectories. A ''quasiperiodic variable'' is a mixture of periodic variables whose periods are not related with rational coefficients. Chaotic trajectories are characterized by an exponential divergence with time of nearby trajectories; because of this, similar system states lead to wildly dissimilar ones later, and so chaotic attractors preclude long-term predictions, a hallmark, or signature, of chaos. As stressed by Glass[14] identifying chaotic trajectories is simple when working with equations, requiring only noting that similar initial conditions are followed by trajectories that, though tending to separate, are statistically similar and within a bounded domain, and then testing whether changing parameters leads to accepted routes to chaos.

In practical application, the state space is an idealized abstraction that may never be known. A system may be composed of an unknown number of coupled variables; one problem, therefore, is deciding a priori which are the relevant ones to observe. Also, it may prove impossible to measure many variables simultaneously. However, an important theorem[69] states that a time-series of just one variable in a dynamically coupled system contains enough information to reveal crucial properties of that system, including an upper bound on the dimensionality of its attractor. The principle behind recovering this information is to construct a mock attractor by embedding an experimentally observed series in a higher dimensional ''phase'' space: the time-series is a trajectory through time of the selected variable. The act of ''embedding'' can be thought of as plotting this trajectory in a phase space whose dimensionality is high enough to prevent the trajectory from intersecting with itself. In other words, if viewed in a phase space of sufficient dimension, the trajectory (and its attractor) would be unique at every point with no ambiguity as to where the system is heading. Conversely, if the embedding is in too few dimensions, the trajectory will intersect with itself, and visualization will lose information about the system's behavior.

A sufficient, but not necessary, condition for a successful embedding is that its dimension $E=2D+1$, where D is the underlying attractor dimension.[63] As an analogy, suppose we wish to embed a one-dimensional piece of string. If the string is straight, all the information about its orientation can be obtained by viewing it in one dimension; if the string connects end to end in a circle, an embedding in two dimensions is sufficient. However, if the string is a tangled mess, one- or two-dimensional embeddings are misleading; think of the shadow cast by the string as an insufficient two dimension embedding. Only viewing the tangled string in three dimensions prevents the erroneous conclusion that it passes through itself; no matter how complicated the tangle, its path can be fully viewed in three dimensions ($E=2\times1+1=3$).

In practice, then, how does one embed the time-series of a variable $X(t)$? The standard method of Takens[69] involves using time-lagged coordinates. First, one chooses an embedding dimension E (we will see ways for evaluating possible choices): let us arbitrarily choose $E=3$ for simplicity. Next, one chooses a time-lag or Δt; let us choose Δt equal to 1, again for simplicity. The embedding is made up of points located in IR^3 as the triplets $[X(t), X(t-1), X(t-2)]$. IR^3 is the Cartesian space with three real-valued dimensions; the generalized j-dimensional vector is $[X(t), ..., X(t-j+1)]$. The embedding process may be visualized as dragging an E-pronged fork along the original time-series with the prongs of the fork separated by Δt. At each position of the fork on the time-series, the tines give the coordinates of an E-dimensional vector whose head is a point in the mock attractor in space; as the fork moves along time, this vector traces the mock attractor. Thus we have used our time-series to create a mapping from the unknown attractor in its unknown space onto a mock attractor residing in phase space. It is this mock attractor which forms a basis for models created to forecast the dynamical system's future behavior. In the present work, the interval order i substitutes for the time-steps used in other applications.

2.2.1 *Dimensionality*. The first practical step is, then, the choice of an appropriate E: it has the obvious limitation that we cannot a priori know D. One possible method involves trial and error testing. Different values of E may be tested by the construction and visual inspection of return maps, the discrete point versions of phase space embeddings. One-dimensional return maps plot one interval against some previous one; the order of the return map is the number of intervals separating them. Return maps of higher dimension contain more axes, each representing another preceding interval. Note that an E-dimensional return map is analogous to an $E-1$-dimensional embedding. For example, the graphs in Fig. 4 plot in two-dimensional space vector $Z_i = (T_i, T_{i-1})$, and are one-dimensional return maps; Fig. 5 contains plots in three-dimensional space (T_i versus T_{i-1} versus T_{i-2}) which are two-dimensional maps; generalized graphs plot in jD space vector $Z_i = (T_i, ..., T_{i-(j-1)})$ and are $(j-1)$-dimensional maps. Figures, judged by the naked eye, tell us if points are dispersed or in clusters (as defined above), if dimensionality affects this and, ultimately, if a particular dimensionality suffices for acceptably resolving the main clusters. Limit cycles generate finite numbers of points, toroidal surfaces generate monotonic curves, and strange attractors generate complicated graphs with extrema that may be multivalued. Noise, ever-present in experimental data, generates unsystematic dispersions. Other features (e.g., precise relations between local densities) relevant elsewhere, are ignored. Computer-controlled displays, viewed from any desired direction, allow precise recognition

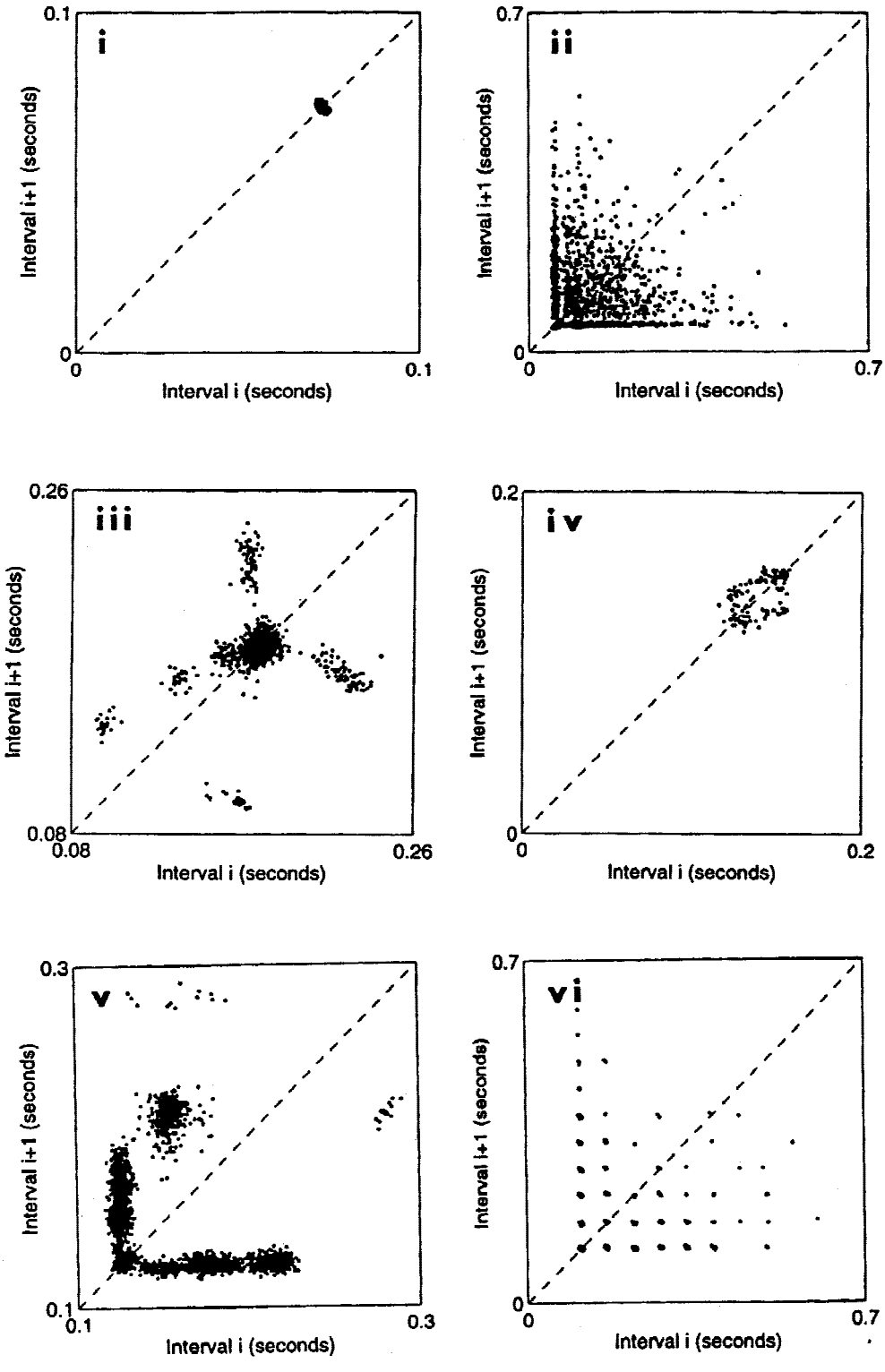
i
0.1
0
0
0.1
Interval i+1 (seconds)
Interval i (seconds)
ii
0.7
0
0
0.7
Interval i+1 (seconds)
Interval i (seconds)
iii
0.26
0.08
0.08
0.26
Interval i+1 (seconds)
Interval i (seconds)
iv
0.2
0
0
0.2
Interval i+1 (seconds)
Interval i (seconds)
v
0.3
0.1
0.1
0.3
Interval i+1 (seconds)
Interval i (seconds)
vi
0.7
0
0
0.7
Interval i+1 (seconds)
Interval i (seconds)

Fig. 4.

of details; however, the same displays presented on two dimensions can be misleading (see Results). ''Poincaré map'' refers to a function expressing one phase in terms of the preceding one (e.g., see Discussion and Refs 16, 17, 20– 22, 36 and 37).

The choice of E is quantified by studying the performance of models based on different embedding dimensions; the most appropriate dimension is inferred from the most successful model. The lagged coordinate reconstruction described above limits us to integer choices of E; in actuality, D itself need not be an integer and, as in fractal ''strange'' attractors, may not be. The models tested are the sequential weighted global linear maps, or S-maps, of Sugihara.[63] These are based on a form of nearest-neighbor algorithm proposed originally by Casdagli,[7] with the future behavior of a ''predictee'' point projected by studying the past behavior of nearby ''predictor'' points in phase space. Prior to model construction, and to minimize nonstationarity, the time-series is first-differenced, i.e. for each value (T_i) is substituted the difference between it and the preceding one ($T_i - T_{i-1}$). Then, the time-series is divided into two parts. The first half is used as a ''known'' past from which a model will be built to forecast the second half, the ''unknown'' future, allowing success to be evaluated out of sample. At this point, we define two neighborhoods, or regions in phase space: one is a ''domain'' neighborhood around the predictee point; the other is an associated ''range'' neighborhood constructed by mapping all the points in the domain one step forward in time. The contribution of each point in the domain neighborhood to the forecast is weighted according to that point's distance in phase space $\mathbb{R}^E$ to the predictee. Since the predictee point will map at time $t+1$ somewhere in the range neighborhood, the latter imposes bounds on our forecast and therefore a first, gross prediction. We shall see momentarily how this forecast is made more precise.

To reiterate, we study the past so as to predict the future. S-maps have two degrees of freedom: the domain neighborhood size and the degree of nonlinearity in the predictor point distance weighting function. It is this distance function that identifies precisely where in the range neighborhood we forecast the predictee to be. Forecasting success for different possible embedding dimensions is evaluated using global linear maps in which the neighborhood is the entire phase space and the distance weighting constant. The dimension of the global linear map which gives the best forecast is judged the best choice of embedding dimension.

Prediction success is evaluated by measuring the agreement between the forecast and actual values in terms of correlation coefficients and errors. Correlation coefficients ρ are the ratios of the covariance between predicted and actual values to the product of the individual standard deviations; ρ were complemented using the z statistic, a transformation applicable when ρ differ from 0. Coefficients were compared using the t-test. Errors are the averages of the absolute values of the differences between actual and predicted values.

2.2.2 *Nonlinearity*. The degree of nonlinearity in the interactions between the system's variables is evaluated after estimating E. Two criteria are applied. (1) One criterion is based on comparison of the predictive successes (judged by correlation coefficients) of the best linear and nonlinear models. Whether coefficients were significantly different was evaluated using the t statistic, smaller than a standard value if the coefficients are equal, and increasing the more they differ: i.e. t estimates are reasonable measures of the magnitude of the linear versus nonlinear difference, and therefore of the degree of nonlinearity. (2) The principle of the second criterion is that the lengths of line segments that provide acceptable piecewise-linear approximations to a given curve vary inversely with the amount of curvature. Accordingly, we expect the quality of the approximation provided by basing forecasts on nearby points to deteriorate with distance from the predictee, linearly in a linear signal, and exponentially if the signal is nonlinear. Domain neighborhood sizes are expressed as proportions of the total number of points. Thus, nonlinearity is explored by evaluating the success of different domain neighborhood sizes for linear maps, and then by employing nonlinear distance weighting functions for global maps. S-maps allow this because they contain a tunable parameter θ (again, see Ref. 67 for the explicit derivation) which allows the degree of nonlinearity in the distance function to be easily

Fig. 4. Two-dimensional return map (order $j=1$). T_i versus T_{i+1} embedding in one dimension. Statistics are in Table 2; the corresponding natural postsynaptic and presynaptic are in Tables 1 and 3. (i) 1:1 locked. Single cluster dispersed around a point, implying that only one interval category can be discerned. Neuron with natural rate 19.14 s^{-1} pacemaker-driven at 14.00 s^{-1} (normalized 0.73); resulting postsynaptic rate 14.00 s^{-1}. Same form but not same trains, as in Fig. 3 and Plate B in Ref. 51 and Figs 3 (later epochs), 5 and 9 in Ref. 52. (ii) Poisson-driven. Points are dispersed, and cluster minimally. Points in a cluster around a point on the diagonal, markedly dispersed throughout, or in elongated clusters parallel to the axes reflect pairs of successive intervals, respectively, without arrivals, irregularly lengthened, or one of each. Sparse bands on either side of the clusters parallel to the axes reflect respectively, refractoriness and minimal lengthenings. Symmetry relative to the diagonal reflects interval serial independence (in this case). Neuron with natural rate 15.3 s^{-1} Poisson-driven at 16.00 s^{-1} (normalized 1.05); the resulting postsynaptic rate was 8.58 s^{-1}. Same form and train as in Fig. 2 in Ref. 55. (iii) Intermittency. Six clusters. Most pairs have almost identical intervals, and produce a cluster around a point on the diagonal; occasional pairs with one or two unusual intervals create point-like or elongated clusters elsewhere. Neuron with a natural rate of 6.73 s^{-1} was driven at a rate of 5.52 s^{-1} (ratio 0.82); the resulting postsynaptic rate was 6.21 s^{-1}. Same form, but not the same trains as in Fig. 5 (later epoch) and Plate C in Ref. 51 and Figs 3 (first epoch), 4B,E and 7 (late epoch) in Ref. 52. (iv) Phase walk through. Points on a rough lozenge whose empty interior and extremes are on the diagonal, the rightmost with the most points. Neuron with a natural rate of 8.5 s^{-1} was driven at a rate of 6.14 s^{-1} (ratio 0.72); the resulting postsynaptic rate was 7.13 s^{-1}. Adapted from, and including the same train as, Fig. 6 and Plate D in Ref. 51. (v) Messy erratic. Four clusters. The vertical or horizontal branches of an ''L''-shaped cluster indicate that natural intervals without inhibition precede or follow lengthened intervals. Three other more or less elongated clusters reflect lengthened interval pairs. Asymmetry reveals serial dependencies. Neuron with a natural rate of 7.84 s^{-1} was driven at a rate of 3.77 s^{-1} (ratio 0.48); the resulting postsynaptic rate was 6.54 s^{-1}. Same form, but not the same trains as in Figs 8, 11 (some epochs) and Plate E of Ref. 51. (vi) Messy stammerings. Many clusters separated by I or a multiple of I form a regular grid. Neuron with a natural rate of 14.4 s^{-1} was driven at a rate of 18.2 s^{-1} (ratio 1.26); the resulting postsynaptic rate was 6.41 s^{-1}. Adapted from, and including the same train as, Fig. 9 and Plate F in Ref. 51.

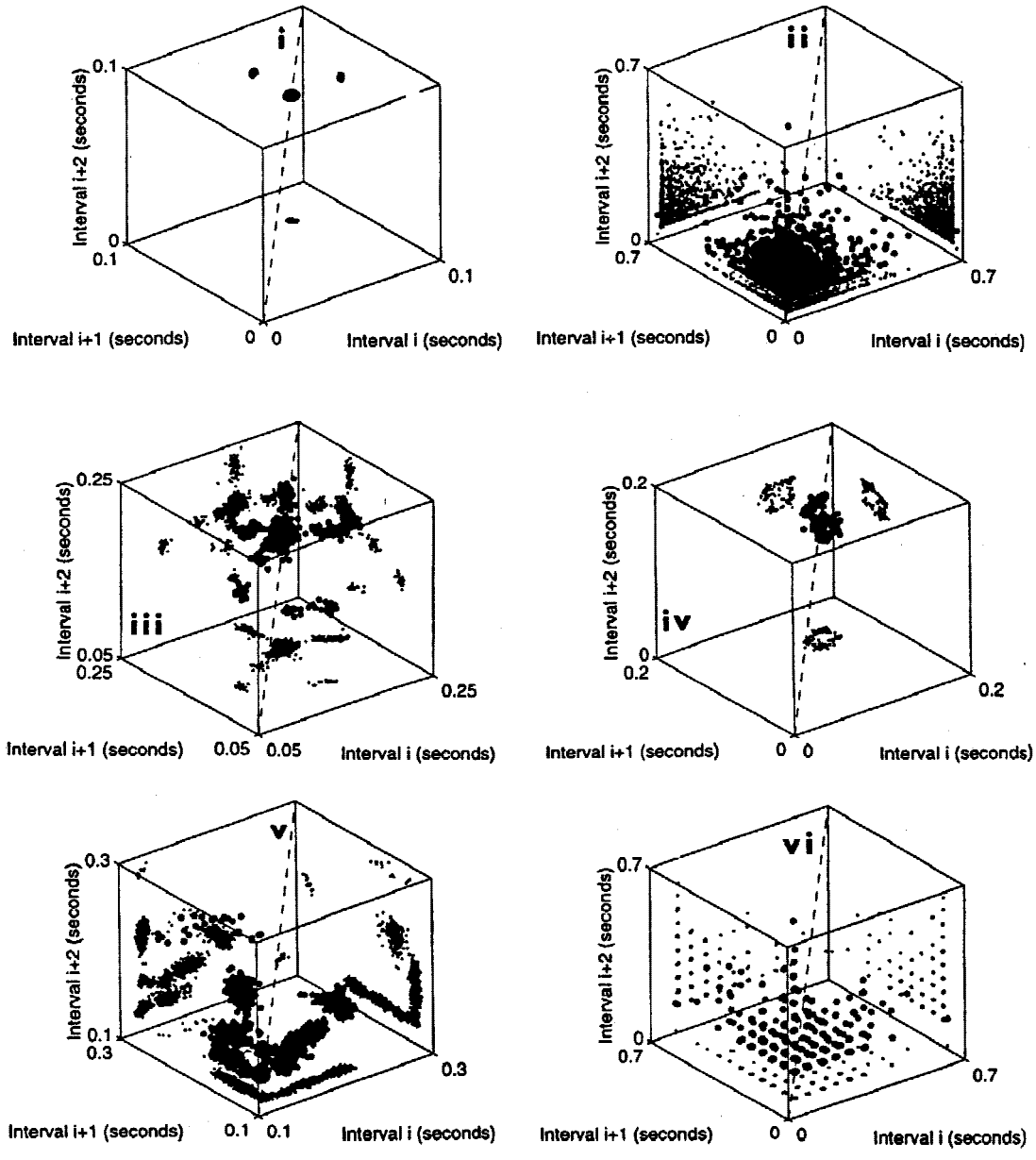

Fig. 5. Three-dimensional return map (order $j=1$). T_i versus T_{i+1} versus T_{i+2}. Embedding in two dimensions. (i) 1:1 locked. Single cluster around a point on the diagonal, implying that only one interval category can be discerned. (ii) Poisson-driven. Numerous dispersed points; clustering only on a point on the diagonal (with coordinates I) and in planes parallel to the reference planes; empty regions along these planes and sparse narrow regions between dispersed and clustered points reflect respectively, refractoriness and minimum lengthenings. (iii) Intermittency. Eight clusters, two more than in two dimensions. (iv) Phase walk through. The number of points is too small to detect structure in three dimensions. (v) Messy erratic. Six or seven clusters. (vi) Messy stammerings. Many clusters separated by multiples of I. Maps of order 1 appear as gray points on the (T_i, T_{i+1}) and the (T_{i+1}, T_{i+2}) planes; a map of order 2 appears as gray points on the (T_i, T_{i+2}) plane. See caption for Fig. 4.

manipulated. Once again, the type of model (global versus local, linear versus nonlinear) which performs best gives insight as to the nature of the underlying system dynamics. ''Global'' or ''local'' means maps based on, respectively, the entire sample or a subset of it.

2.2.3. *Predictability*. The argument is expressed in terms of numbers of intervals and not of time-spans: i.e. reflects the point process evolution along order and not along time. The expression ''prediction time'' used in earlier publications is retained because it still refers to forecasting the future.

We are now in a position to observe how model forecasting success (evaluated by correlation coefficients and errors) changes with increasing prediction times—i.e. numbers of intervals—by simply iterating the steps described above and obtaining predictions multiple steps into the future. We call the time-span or the number of intervals into the future over

which models give the best predictions the ''forecast horizon''. Prediction success—or failure—can be the same everywhere into the future, i.e. error constant with prediction time. This invariant predictive power is alluded to as a ''long horizon'': it means that errors are caused by an additive noise uncorrelated with the process itself; such noise may reflect measurement error or unknown higher-order system dynamics. Alternatively, prediction can deteriorate as time progresses, i.e. errors increase. A declining predictive power is called ''short horizon'': it hints strongly of complex deterministic dynamics that reveal themselves in the near future but, relating to a sensitivity to initial conditions, deteriorate beyond and lead to chaos. The future may to some extent be predicted from the behavior of past values that are similar to those of the present. Short horizons can appear also with certain largely random dynamics such as colored noise.[14] Finally, between the long and short horizons, there exists a continuum wherein distinctions are blurred in any practical sense.

Dimensionality, nonlinearity and predictability allow full investigation of Sugihara and May's three-way operational definition of chaos.[67] The presence of chaotic behavior is strongly suggested if the following criteria are met: (i) an optimal low dimension model, (ii) a strong nonlinearity, and (iii) a short forecast horizon. Identifying chaotic trajectories is relatively simple when working with equations, but uncertain when dealing with experimentally collected time-series where current techniques (spectra, dimension, Lyapunov exponents, predictability) are individually insufficient.[14]

Once identified rigorously by dimensionality, nonlinearity, and forecast horizon, each spike train form can be matched more reliably with the theoretical considerations; the latter's broader and detailed descriptions contribute significant insights about the dynamics of pacemakers driving pacemakers (see Discussion).

3. RESULTS

The distinctive qualities of each form are illustrated in Fig. 2 by basic graphs of postsynaptic intervals along time. As explained (Experimental Procedures), every train analysed here, selected from a broader set reported earlier, was typical of a particular form.[29,51,52,55] In Fig. 2i, all points are in a vertically tight cluster that extends horizontally throughout the graph, as it does throughout the stationary sample the panel represents. Their ordinates, all practically the invariant inhibitory interval *I*, mean that all postsynaptic intervals are equal to *I*. It illustrates the periodic form called 1:1 locking, where one presynaptic and one postsynaptic spike alternate with invariant phases. This form is driven by pacemaker patterns whose averages (rate, interval) are close to the natural postsynaptic values. More generally, *p:q* lockings are repetitions of sets of *p* presynaptic intervals, *q* postsynaptic intervals and *q* phases; the *q* postsynaptic intervals are not necessarily the same but exhibit an invariant order or pattern (as do the phases); lockings other than 1:1 were not subjected to nonlinear analyses.

A Poisson-driven form is in Fig. 2ii. Points fall into two categories. Some are in a vertically tight cluster that extends horizontally throughout both figure and the train it represents; its ordinate is practically the natural postsynaptic interval *N*. The other points are above and dispersed irregularly, their density decreasing upwards monotonically and continuously. The two categories reveal postsynaptic intervals that, respectively, do not contain inhibitory arrivals and are close to *N*, or contain arrivals and are lengthened. Because arrivals are Poisson-driven, the postsynaptic interval sequence is largely unpredictable. The sparse band just above *N* reflects the known fact that there is a minimum, non-zero lengthening.[29,42,48] Poisson-driven trains are driven by Poisson patterns at any average rate. As rates increase, postsynaptic intervals tend to be longer, the proportion of natural intervals falls, and forms approach low rate Poisson processes.

The remaining forms are pacemaker-driven. In Fig. 2iii, points fall into two categories. A large majority are in a vertically tight cluster that extends practically horizontally throughout; their ordinates are almost the invariant inhibitory interval *I*. In addition, and breaking up the horizontal cluster, a few points compose brief and variable vertical groups or ''bursts'': these arise sporadically, i.e. rarely and at irregular intervals. This form is mostly regular and predictable, but irregularizes briefly in a manner that is unpredictable, both as to when bursts happen and to their intrinsic details. Time-series with these features have been called ''intermittent'' (see Discussion).[3,4,14] This intermittent character was the prevalent feature of these basic graphs when their build-up was followed slowly point by point (see Experimental Procedures); present too, but clearly less apparent was some hard to describe and summarize irregularity, i.e. some messiness (see below). The regular portions are occasionally alluded to as ''stable'' and the bursts as ''destabilizations'': terms are descriptive, not implying rigorous tests of resistance to perturbations.

The train in Fig. 2iii, which is consistent with the requirements of prevalent regularity plus brief sporadic irregularization established for intermittencies, includes, as demonstrated below, a significant chaotic contribution (of the sort that characterizes the train in Fig. 2v labelled erratic). The concepts of intermittency and chaos are not mutually exclusive and, therefore, a train can simultaneously be intermittent and chaotic: this issue arises also below and is pursued in the Discussion.

Figure 2iv also shows an essentially horizontal cluster (curved arrow) broken up by vertical groups (vertical arrow), and can be considered intermittent. It is a special intermittency, however, for the predominance of the horizontal, strongly predictable portions is only slight and the irregularity within bursts and in between-burst intervals is weaker. Furthermore, the phases (illustrated in Fig. 7B in Ref. 51 but not here) sweep their range monotonically in a manner that, as can be appreciated better in the phase basic graphs, is partly predictable: this led to their designation as ''phase walk throughs''.[12] In terms of overall regularity, the brevity of the regular portions is compensated by a

repetitiveness that involves the entire postsynaptic train and the phases.

Experiments repeatedly demonstrate that the stationary portions of walk throughs last substantially less than those of other forms (see Discussion).[51,52] Though rigorous tests of resistance to perturbations have not been performed, this is interpreted as meaning that walk throughs are the least stable in the face of inevitable ongoing perturbations.[57] Because of this, stationary samples did not suffice for significant nonlinear estimates, and were omitted from Tables 4–7. Stationarity refers to trains being trend-free (Experimental Procedures), and does not imply whether, in the senses explained above, local regular or irregular portions are stable or unstable, respectively.

Figure 2v and vi correspond to inhibitory rates lower and higher, respectively, than those eliciting 1:1 lockings. These trains, called ''messy'', are hard to summarize, and lack easily predictable orderings. Fig. 2v shows a messy ''erratic'' train. Points are in horizontal clusters that extend throughout. The lower one, whose ordinate is N, corresponds to intervals that do not contain inhibitory arrivals and are practically unmodified. Only this cluster, the most restricted vertically and with the highest density and sharpest boundaries, stands out clearly. The remaining clusters are above it, and represent intervals lengthened by arrivals; all (except the top one with few points) are less restricted vertically and have lower densities and greater dispersions, merging with one another. Clusters represent favored interval values but points elsewhere, i.e. other intervals, are relatively common. The sparse band between the lowest clusters reflects the minimum lengthening (see Fig. 2ii).[29,42,48] The prevalent feature when following the basic graph as it was built up slowly was a marked difficulty in describing and summarizing its evolution, i.e. its messiness. Hence, even though pacemaker arrivals are regular and predictable, this postsynaptic sequence is irregular and largely unpredictable.

Windowing appears when the invariant pacemaker interval I is shorter than the natural postsynaptic interval N. In ''windowing'', postsynaptic spikes occur only around the driver spike: hence, each postsynaptic interval is between two spikes that are each associated with a driver spike and which bracket one or more of these. Consequently, postsynaptic intervals are multiples of I, and phases (not shown) are almost either I (1, if normalized to I) or 0.[51] Depending on I (or, rather, on N/I), windowing involves $p1$ lockings ($p=2, 3,...$), intermittencies or, when sequences are very unpredictable, ''stammerings'' (a term coined because of how spike trains sound over an audio system). Windowing is also called ''skipping'' because postsynaptic spikes skip certain driver periods (regularly or irregularly).[31,32,43] Figure 2vi shows stammering. Points are in vertically tight clusters that, though interrupted irregularly, extend horizontally throughout the graph and the stationary sample. The ordinates of all clusters are multiples of the inhibitory interval I (horizontal arrow), i.e. $2I$, $3I$, etc. In stammerings, points skip from one cluster to the next in a largely unpredictable order.

The quantitative summary of timing was achieved with several statistics, of which some, alluding to dispersion and sequence (i.e. pattern), are critical for form diagnosis; described and illustrated fully in the earlier publications, they are only summarized here.[51] The conventional statistics of the trains in the figures are in their respective legends and Table 2; corresponding natural and presynaptic ones are in Tables 1 and 3, and were complemented by interspike interval histograms. Second-order statistics, such as autocorrelation histograms, autocorrelation sequences and spectra (in Hz or cycles/order), provide information about the trains' periodicities and predictabilities: the absence of peaks and troughs or, when present, their magnitudes, locations and separations, revealed the following. $p:q$ lockings are strongly periodic and very predictable with periods equal to the span of the repeating set of p presynaptic and q postsynaptic intervals in the time-domain or to q in the serial order domain. Only 1:1 lockings where $p=q=1$ were analysed here: accordingly, their periods are equal to I or to 1, spectra either have outstanding peaks at I^{-1} (and harmonics) when in Hz or are flat in cycles/order (because all serial correlation coefficients are equal). The spectra of Poisson-driven forms have a peak reflecting the unperturbed intervals and are largely uniform, i.e. noisy, elsewhere: peaks decrease and noise increases as arrival rates increase. Intermittencies have periodicities plus background noise in different degrees. Messy forms have weak periodicities plus a strong background noise.

3.1. *Nonlinear analysis*

3.1.1. *Dimensionality*. Table 4 has several portions, one for each form; each has a dimension in each row and a neighborhood size in each column. Again, models are evaluated by correlation coefficients between predicted and out of sample observed values. Thus Table 4 summarizes the success in forecasting the different forms of global linear models with different choices of embedding dimension E. In most trains and forms, as E increases with any given neighborhood size (i.e. down any given column), coefficients increase and then plateau: for example, for locked (i) and in the rightmost column (neighborhood 822), values are 0.430 at $E=1$, increase monotonically, reach 0.590 at $E=5$ (four dimensions), and stay high thereafter; for erratic (v) and down an intermediate column (128), coefficients increase monotonically, reach 0.756 at $E=6$ (five dimensions); both stay high up to $E=7$ (six dimensions). Figure 3, with correlation coefficients against E, illustrates this

Table 4. Correlation coefficients ρ between actual and predicted values at given dimensionalities *E* (1, 2,...) across each row, and given neighborhood sizes *b* (32, 45,...; values chosen arbitrarily) down each column. Each entry is the highest obtained with those *E* and *b*. The smaller the neighborhood, the more nonlinear the case. Here, as in all tables, spike train forms are (i) 1:1 locking, (ii) Poisson-driven, (iii) intermittent, (v) messy erratic, (vi) messy stammering

i. Locked 1:1

E	32	45	64	91	128	181	256	362	512	724	822
1	0.423	0.426	0.429	0.428	0.430	0.431	0.431	0.428	0.429	0.429	0.430
2	0.493	0.501	0.513	0.509	0.507	0.512	0.515	0.516	0.516	0.520	0.521
3	0.511	0.521	0.527	0.524	0.529	0.528	0.533	0.539	0.543	0.545	0.546
4	0.539	0.545	0.554	0.552	0.557	0.568	0.572	0.577	0.581	0.583	0.585
5	0.503	0.533	0.541	0.559	0.567	0.575	0.575	0.584	0.586	0.588	0.590
6	0.543	0.555	0.568	0.569	0.573	0.583	0.588	0.592	0.597	0.600	0.602
7	0.538	0.567	0.579	0.571	0.586	0.588	0.592	0.595	0.598	0.605	0.606

ii. Poisson-driven

E	32	45	64	91	128	181	256	362	512	724	1024	1448	2048	2544
1	0.311	0.308	0.325	0.336	0.340	0.341	0.337	0.335	0.336	0.331	0.325	0.308	0.175	0.133
2	0.330	0.332	0.347	0.354	0.360	0.359	0.362	0.362	0.362	0.361	0.349	0.263	0.205	0.166
3	0.334	0.345	0.350	0.363	0.368	0.370	0.376	0.377	0.376	0.370	0.355	0.286	0.231	0.196
4	0.310	0.343	0.355	0.362	0.366	0.378	0.382	0.378	0.376	0.371	0.357	0.294	0.244	0.206
5	0.323	0.334	0.350	0.361	0.375	0.381	0.381	0.380	0.381	0.375	0.364	0.280	0.232	0.213
6	0.296	0.315	0.331	0.354	0.364	0.367	0.365	0.365	0.365	0.368	0.358	0.279	0.242	0.232
7	0.274	0.300	0.315	0.330	0.341	0.351	0.355	0.356	0.362	0.367	0.353	0.273	0.246	0.245

iii. Intermittent

E	32	45	64	91	128	181	256	362	512
1	0.434	0.439	0.450	0.452	0.450	0.454	0.450	0.446	0.442
2	0.504	0.513	0.509	0.521	0.518	0.513	0.505	0.483	0.462
3	0.519	0.504	0.502	0.517	0.515	0.506	0.491	0.473	0.460
4	0.510	0.501	0.524	0.500	0.489	0.474	0.464	0.467	0.457
5	0.447	0.431	0.415	0.447	0.477	0.461	0.471	0.462	0.455
6	0.445	0.447	0.448	0.425	0.428	0.434	0.432	0.425	0.421
7	0.399	0.383	0.368	0.356	0.388	0.426	0.431	0.424	0.435

v. Messy erratic

E	32	45	64	91	128	181	256	362	512	724	1024
1	0.574	0.580	0.579	0.583	0.584	0.583	0.581	0.573	0.553	0.528	0.425
2	0.673	0.681	0.681	0.681	0.679	0.676	0.672	0.663	0.638	0.610	0.502
3	0.730	0.734	0.737	0.737	0.733	0.731	0.725	0.716	0.668	0.637	0.576
4	0.722	0.733	0.740	0.743	0.741	0.738	0.732	0.721	0.681	0.635	0.574
5	0.730	0.739	0.747	0.753	0.751	0;749	0.740	0.725	0.679	0.644	0.611
6	0.727	0.739	0.752	0.754	0.756	0.752	0.747	0.727	0.666	0.642	0.614
7	0.712	0.737	0.748	0.753	0.757	0.744	0.740	0.727	0.658	0.645	0.629

vi. Messy stammering

E	32	45	64	91	128	181	256	362
1	0.002	0.007	0.014	0.025	0.037	0.039	0.015	0.008
2	−0.0l3	−0.004	−0.020	0.014	0.011	0.020	0.006	0.041
3	0.042	0.019	−0.015	0.005	0.021	0.027	0.036	0.037
4	0.038	0.059	0.067	0.061	0.019	0.020	0.011	0.006
5	0.069	0.060	0.077	0.031	0.018	0.023	0.029	0.003
6	0.067	0.077	0.043	0.034	0.020	0.009	0.024	−0.028
7	0.037	0.033	0.016	−0.007	−0.011	−0.001	−0.034	−0.039

Table 5. Comparison of nonlinear and linear models. Nonlinear models are no better than linear ones for lockings, better for the Poisson-driven, intermittent and erratic forms; differences are marginal for stammerings. ρ, correlation coefficients; *z* statistics, more generally applicable transformation of ρ; difference of *z* in the nonlinear minus the linear model of the same train; *t*-test, evaluates the difference between correlation coefficients. Significant values for *t* at the 97.5% (0.025) level are over 2.000, 1.980 or 1.960 for sample sizes of 60, 120 or larger, respectively. The dimensionality for all cases is the optimal one for the nonlinear models

Form	Sample size	Nonlinear ρ	Nonlinear *z*	Linear ρ	Linear *z*	Δ*z*	*t*-test
i. Locked 1:1	823	0.585	0.670	0.585	0.670	0.000	0.000
ii. Poisson-driven	2545	0.377	0.397	0.206	0.199	0.198	7.059
iii. Intermittent	1201	0.524	0.578	0.175	0.177	0.401	9.812
v. Messy erratic	2591	0.753	0.980	0.529	0.589	0.391	14.068
vi. Messy stammering	722	0.077	0.077	−0.023	−0.023	0.100	1.899

Table 6. Sample sizes, embedding dimensions (approximate) and neighborhood size (relative to the total sample) that allow the best fit

Discharge form	Sample size	Embedding dimension	Neighborhood size as proportion of sample
i. Locked 1:1	823	5	1.000
ii. Poisson-driven	2545	4	0.142
iii. Intermittent	1201	3	0.076
v. Messy erratic	2591	5	0.035
vi. Messy stammering	722	5	0.089

prevalent evolution of prediction success for a locked (open circles) and an erratic (crosses) form.

In some trains, coefficients decline significantly at high E. For example, for the Poisson-driven train (ii) this happens for most neighborhood sizes (for 12 out of 14 of them; only the two rightmost columns are excepted): in central column 181 (illustrated by Fig. 3 pluses), say, values are 0.341 at $E=1$, increase to 0.381 at $E=5$ (four dimensions), and then decrease to 0.351 at $E=7$ (six dimensions). This can also occur for other forms. Sugihara and May[67] tentatively attribute this counterintuitive finding to contamination by Z_i points whose remoter coordinates (further back in time) are similar to those of the predictee, but whose recent coordinates are less similar.

Figures 4 and 5 are two- and three-dimensional return maps. Points for 1:1 lockings (Figs 4i, 5i) form a single tight cluster around a point on the diagonal. A good fit is a monotonic function whose stable intersection with the diagonal attracts all iterated points. The fit is ''invertible'' because a unique T_{i+1} corresponds to each T_i and vice versa. This suggests that fits to the one-dimensional map would suffice for satisfactory modeling (see Discussion). Correlation coefficients (Table 4i, Fig. 3, small circles) indicate that at any given neighborhood size (i.e. column) practically all additional dimensions add some improvement, with acceptable values for $E=5$ (four-dimensional maps): this suggests five and thus four dimensions as a reasonable cut-off for models. Coefficients continue to increase, however, and $E=6$ (five dimensions) could be an alternative, not unreasonable cut-off.

Poisson-driven spike trains (Figs 4ii, 5ii) show points clustered around a point on the diagonal, clustered around lines parallel to the axes, clustered around planes parallel to the reference planes, or distributed irregularly: they reflect intervals, respectively, all without arrivals (unperturbed), only one unperturbed, only one lengthened or all lengthened. Clusters become sparser when arrival rates increase, and unperturbed intervals are less likely. Table 4ii, indicates that in most neighborhood sizes (only two columns, the rightmost, are excepted), each additional dimension (increasing downwards) adds some improvement, but only up to a certain dimensionality after which predictions deteriorate. For example, at the intermediate column 181, values are 0.341 for $E=1$, reach 0.381 for $E=5$ (four dimensions) and decay to 0.351 for $E=7$ (six dimensions). Correlation coefficients indicate that dimensionality is only mildly influential; keeping this in mind, acceptable predictions suggest an E between 4 and 5, and thus an approximately three- to four-dimensional attractor.

In intermittencies (Figs 4iii, 5iii), points are separated into six clusters in a one-dimensional map but several more in the two-dimensional map. This suggests that fits to the one-dimensional map would not suffice for satisfactory modeling (see Discussion). Coefficients (Table 4iii) suggest that an E around 4 is satisfactory. Correlation coefficients for the case in Table 4iii indicate that, at all neighborhood sizes (columns), additional dimensions improve predictions. For example, at neighborhood 32 (leftmost column), values are 0.434 for $E=1$, reaching 0.519 for

Table 7. Prediction times T_P from 1 to 10 for each form (whose sample size, dimension and neighborhood size are included). Errors and correlation coefficients ρ involving the actual values and those predicted by the non-parametric method. Probability that ρs equal 0, i.e. that there is no evidence that correlations exist and therefore that models are successful (rightmost column): low or high values point to predictions that, respectively, are reliable or unreliable

Discharge form	Sample size	Embedding dimension	Number of neighbors	Prediction time	Error (ms)	Correlation coefficient	P ($\rho=0$)
			822	1	0.477	0.585	0.0000
		821	2	0.591	0.093	0.0037	
		820	3	0.594	0.063	0.0358	
		819	4	0.593	0.060	0.0428	
		818	5	0.593	0.044	0.1025	
i. Locked 1:1	823	4	817	6	0.595	−0.014	0.6554
		816	7	0.596	−0.053	0.9334	
		815	8	0.596	0.018	0.3017	
		814	9	0.597	0.020	0.2858	
			813	10	0.596	0.029	0.2056
			1	36.597	0.377	0.0000	
			2	36.643	0.382	0.0000	
			3	36.444	0.385	0.0000	
			4	36.467	0.385	0.0000	
			5	36.661	0.380	0.0000	
ii. Poisson-driven	25454	362	6	36.717	0.383	0.0000	
			7	37.032	0.374	0.0000	
			8	37.182	0.369	0.0000	
			9	36.965	0.374	0.0000	
				10	36.964	0.374	0.0000
			1	8.107	0.522	0.0000	
			2	8.957	0.303	0.0000	
			3	9.598	0.066	0.0108	
			4	9.829	0.064	0.0138	
iii. Intermittent	1201	3	91	5	10.003	0.106	0.0001
			6	10.117	0.106	0.0001	
			7	10.088	0.107	0.0001	
			8	10.086	0.024	0.2057	
			9	10.022	−0.023	0.7885	
				10	9.974	−0.013	0.6777
			1	11.886	0.753	0.0000	
			2	15.223	0.634	0.0000	
			3	18.082	0.569	0.0000	
			4	18.897	0.551	0.0000	
			5	20.086	0.520	0.0000	
v. Messy erratic	2591	5	91	6	21.789	0.444	0.0000
			7	23.129	0.368	0.0000	
			8	24.530	0.285	0.0000	
			9	24.962	0.272	0.0000	
				10	25.361	0.253	0.0000
			1	60.554	0.585	0.0191	
			2	61.787	0.093	0.4963	
			3	62.473	0.063	0.8218	
			4	60.885	0.060	0.9720	
			5	62.205	0.044	0.9985	
vi. Messy stammering	722	5	64	6	61.687	−0.014	0.9316
			7	60.933	−0.053	0.3519	
			8	62.078	0.018	0.7336	
			9	62.112	0.020	0.8070	
				10	62.717	0.029	0.9916

$E=3$, Acceptable values are achieved for $E=3$, 4 (two-, three-dimensional maps): this suggests a reasonable cut-off of around three dimensions. Improvement happens only up to a point, beyond which deterioration occurs (as for the Poisson-driven case, see above), falling to 0.399 for $E=7$ (six dimensions). In this and other respects, intermittent trains were the least uniform of all, resembling locked trains, erratic ones, or being somewhere in between: this reflects the relative prevalence of their regularities (see Discussion). In phase walk throughs, in two dimensions (Fig. 4iv) interval points follow quite closely a closed one-dimensional curve that intersects the diagonal, leaving a broad interior devoid of points. The non-invertibility of this map disappears if data are plotted with polar coordinates whose origin is inside the curve.[38] In three dimensions (Fig. 5iv), points follow a one-dimensional open curve that is close to the diagonal but does not touch it; because it winds around the diagonal, this display appears as a fuzzy point. Phase maps (see Fig. 6E in Ref. 51) have in two dimensions an elongated cluster well fitted by an invertible monotonic one-dimensional curve. Walk through maps suggest that approximations to

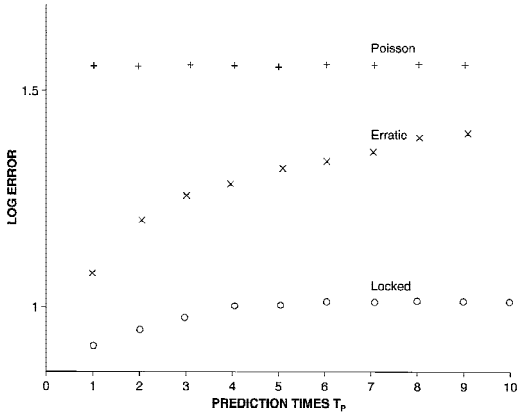

Fig. 6. Logarithm of errors, prediction times and form. ''Prediction time'' T_P is a number of forthcoming intervals. The ''forecast horizon'' is the number of such intervals that can be predicted acceptably. Open circles, 1:1 locking: errors are small at short T_P and then increase moderately. Neuron with natural rate 19.14 s^{-1} pacemaker-driven at 14.00 s^{-1} (normalized 0.73); resulting postsynaptic rate 14.00 s^{-1}. Pluses, Poisson-driven: errors about equally high at all T_P. Neuron with natural rate 15.3 s^{-1} Poisson-driven at 16.00 s^{-1} (normalized 1.05); resulting postsynaptic rate 8.58 s^{-1}. Crosses, erratic: errors are small at short T_P and then increase markedly. Neuron with natural rate 7.84 s^{-1} pacemaker-driven at 3.77 s^{-1} (normalized 0.48); resulting postsynaptic rate 6.54 s^{-1}. Comparable plots for intermittencies (not depicted) resemble either the locked or the erratic ones; stationary samples from phase walk throughs were not large enough to justify conclusions. Additional statistics are in Tables 1–3.

the one-dimensional map (of phases particularly) would lead to satisfactory modeling (see Discussion).

In erratic spike trains (Figs 4v, 5v), points form four clusters in a one-dimensional map, but again much greater structure is revealed in the two-dimensional map. This suggests that fits to the one-dimensional map would not suffice for satisfactory modeling (see Discussion). Intermittent and erratic trains, though having clearly different basic graphs and two-dimensional return maps (Figs 2iii,v, 4iii,v), have three-dimensional return maps that seem rather similar to the naked eye (Fig. 5iii,v). Complete similarity is only apparent, however; the figure failing to illustrate clearly important differences that can be appreciated by computer-controlled rotation of the display, most notably that the intermittent form has most points in a dense cluster practically on the diagonal. Correlation coefficients for erratic forms (Table 4v, Fig. 3, crosses) indicate that additional dimensions improve predictions at all neighborhood sizes (columns). For example, at neighborhood 128, values are 0.584 for $E=1$, and increase monotonically up to 0.757 for $E=7$ (six dimensions). Acceptable values are achieved generally around $E=6$ (five-dimensional maps): this suggests a reasonable cutoff around five dimensions.

With stammerings (Figs 4vi, 5vi), points form clusters on a grid whose nodes are separated by multiples of I. The number of clusters increases with dimensionality (while the number of points per cluster decreases). Correlation coefficients (Table 4vi), though very small, suggest that an E around 5 or 6 satisfactorily discerns the main clusters.

3.1.2. *Nonlinearity*. The respective successes of nonlinear and linear models are compared for each form (at the optimal dimensionality for the nonlinear models) in Table 5. The most successful model is that which allows better predictions, as judged by coefficients ρ and z (a more broadly applicable version of ρ) between actual and predicted values (Experimental Procedures). Coefficients (central columns) were larger for nonlinear than for linear models in all forms except lockings.

Coefficients were compared using the t statistic (rightmost column): they are significantly different at the 97.5% level and for the sample sizes used (leftmost column), when t is over 1.960. Furthermore, the larger t is, the greater the differences between the coefficients and between the models. Hence, t measures the form's degree of nonlinearity. Table 5 indicates that ρs are clearly different for Poisson-driven, more so for intermittent, and maximally so for the erratic forms; coefficients are not significantly different for lockings, and just under significance for stammerings. Hence, data are respectively compatible with nonlinearities of different magnitudes, compatible with linearity, and inconclusive.

Results in Table 4 are also relevant to the issue of linearity vs nonlinearity. As pointed out above, each portion lists ρs for a different form (see above), each row representing a dimension E and each column a neighborhood size b. Neighborhood size, which increases rightwards along each row (i.e. for a particular dimension), provides the second criterion for evaluating the degree of nonlinearity (Experimental Procedures): the principle is that the greater the curvature, the shorter the segments of the best piecewise-linear approximations. Domain neighborhood sizes are expressed as proportions of the total number of points, and are particularly significant at the E that corresponds to dimension assigned to the form (see above). For lockings and regardless of dimension (i.e. row), coefficients always are the lowest at the smallest (leftmost) neighborhood and highest at the largest (rightmost) neighborhood: increases in between are monotonic or almost. The rows for the most acceptable dimensionalities of four dimensions or five dimensions ($E=5$, 6) are completely monotonic. For Poisson-driven, intermittent and erratic forms and regardless of dimension, coefficients first increase, reach a maximum in some intermediate neighborhood (column), and then decrease. For the Poisson-driven form, say, across row $E=5$ of its assigned four dimensions, ρs start at 0.323 with neighborhood 32, peak at 0.381 at 181 and then drop to 0.213 at the last column with neighborhood 2544. The small ρs for stammerings do not

allow definitive conclusions. Hence, best linear fits involve the entire sample for lockings, and smaller portions for Poisson-driven, intermittent or erratic forms. The inference is that only lockings are compatible with linear models. Table 6 shows in the rightmost column for each form and its assigned dimensionality the neighborhood size expressed as a proportion of sample size.

3.1.3. *Predictability*. Table 7 lists, for each form and along increasing numbers of subsequent intervals $T_P = 1,...,10$, error, ρ, and probability of ρ being 0; integers T_P are called ''prediction times''. The evolution of the errors along T_P, in the sense of whether they are invariant or increase (i.e. of whether long or short prediction horizons exist) is critical, regardless of error magnitudes (Experimental Procedures). The evolution of the errors was complemented by those of the correlation coefficients and of the probabilities that $\rho = 0$. The event of $\rho = 0$ is equivalent to there being no correlation between actual and predicted values, and of complete prediction failure. Hence, higher probabilities go with weaker correlations and worse predictions; lower probabilities go with stronger correlations and better predictions.

The evolution of the errors is detailed in Table 7. Two extreme evolutions—long and short horizons—are possible, each characterizing particular dynamic behaviors. In long horizons, errors are essentially invariant at all steps along T_P, i.e. prediction horizons are long: this holds for locked, Poisson-driven and stammering trains. Long horizons suggest uncorrelated, additive noise, which, in the noted absence of significant measurement error, reflects some unknown higher-order system dynamic. Long horizons can involve different kinds of uniform predictability. The evolution of the locked train (open circles in Fig. 6) involves small errors: indeed, all are around 0.5 ms, and far below the range of the intervals (in fact barely above the 0.3 ms measurement errors). Small errors, reflecting small differences between actual and predicted values, are compatible with the small correlation coefficients (absolute values under 0.1) reflecting lack of correlation between departures from the mean. The step 1 error (0.477) is smaller than subsequent ones, and its correlation coefficient (0.585) is the only one that differs significantly from 0: hence, some additional predictability exists from one interval to the next, a feature shared by most trains analysed, regardless of form. Contrastingly, the long horizon of the Poisson driven train (Fig. 6, plusses) involves larger errors: all are around 37.0 ms, and in the range of the intervals. The correlation coefficients are around 0.3 and, with a (practically) zero probability of being equal to 0, are significantly different from 0: this implies that a weak predictability exists throughout. Stammerings (not included in the figure) have large errors around 61.0 ms and low correlation coefficients (under 0.09) with high probabilities of being equal to 0.

In short horizons, errors are initially small but increase with T_P (Table 7v, Fig. 6, plusses): hence, predictions are accurate initially and decay along T_P, i.e. have short horizons. The erratic train has errors that start at their lowest value (11.886) for step 1, and then increase unceasingly, particularly up to, say, step 7 (23.129). Likewise, correlation coefficients start at the highest value (0.753) at step 1, and then decrease unceasingly. Correlation coefficients are throughout over 0.253, and their null probabilities of being 0 indicate that all differ significantly from 0. A short horizon is equivalent to sensitivity to initial conditions, and is one of the criteria needed for signals to be considered potentially chaotic. The intermittent train represented in tables and figures also has a short horizon: errors start at their lowest value (8.107 ms) for step 1, increase, reach high values at step 6 (10.117 ms) and subsequently maintain them; at steps 1 and 2, the correlation coefficients are high (0.522, 0.303) and their null probabilities of being 0 indicate that they differ significantly from from 0.

As noted above, intermittent trains varied: they became less like erratic trains and more like periodic locked trains as their regular portions became more prevalent. Some intermittencies may have horizons intermediate between the extreme categories illustrated here. Thus, horizons comprise a continuum in whose extreme and intermediate portions form classification can be performed with, respectively, assurance or uncertainty.

Figure 6, where errors are logged on the ordinate, illustrates typical cases of the extreme evolutions: namely, on the one hand those with long horizons by either lockings with small errors (open circles) or Poisson-driven with large errors (pluses); on the other, those with short horizons by the erratic train (crosses). Such displays allow summarization of the error's evolution with T_P by the slope in the region of the logarithm's growth prior to the eventual plateau; in Fig. 6 and for the erratic train, this region is from $T_P = 0$ to $T_P = 4$.

Figure 7 ranks forms by nonlinearity and predictability. Nonlinearity (on the abscissa) is quantified by the t statistic that evaluates nonlinearity by the difference between linear or nonlinear models as in Table 5. Predictability (ordinate) is quantified by the maximum slope of the error's logarithm in plots as those in Fig. 6. Spike trains with different forms have different positions. The periodic lockings (open circle) are linear with gentle slopes (long horizons), and thus located at the lower left; stammerings (star) are marginally linear with long horizons and thus close by. Poisson-driven forms (plus), nonlinear with gentle slopes (long horizons), are represented at an intermediate position on the abscissa's axis. Erratic train (cross), nonlinear with steep slopes (short horizons), are located on the upper right. Intermittencies, depending on the preponderance of their regularities and irregularities, can be closer to either the locked

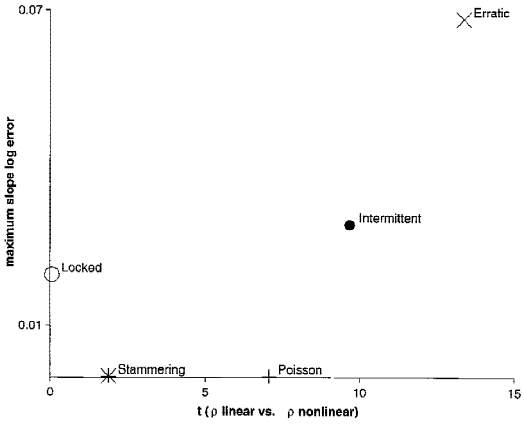

Fig. 7. Nonlinearity, prediction time and form. Point position reveals jointly the nonlinearity and predictability of each form. Abscissa: t value that compares the correlation coefficients achieved by linear and nonlinear predictions, and when larger reflects greater nonlinearity. Ordinate: slope of the plot in Fig. 6 (with logarithm of error vs T_P), and larger for faster prediction deterioration. Their statistics are in Table 2; the corresponding natural postsynaptic and presynaptic are in Tables 1 and 3. Open circle, 1:1 locked: linear with (small) errors that increase little. Neuron with a natural rate of 19.14 s^{-1} pacemaker-driven at 14.00 s^{-1} (normalized ratio 0.73); the resulting postsynaptic rate was 14.00 s^{-1}. Same form but not same trains, as in Fig. 3 and Plate B in Ref. 51 and Figs 3 (later epochs), 5 and 9 in Ref. 52. Plus, Poisson-driven: intermediate nonlinearity and negligible slope. Neuron with natural rate 15.3 s^{-1} Poisson-driven at 16.00 s^{-1} (normalized 1.05); the resulting postsynaptic rate was 8.58 s^{-1}. Same form and train as in Fig. 2 in Ref. 55. Black circle, intermittent: the case represented has significant values in both respects; other intermittencies may be closer to either lockings or erratic trains. Neuron with a natural rate of 6.73 s^{-1} was driven at a rate of 5.52 s^{-1} (ratio 0.82); the resulting postsynaptic rate was 6.21 s^{-1}. Same form, but not the same trains as in Fig. 5 (later epoch) and Plate C in Ref. 51, and Figs 3 (first epoch), 4B,E and 7 (late epoch) in Ref. 52. (Phase walk throughs, whose stationary samples were not large enough to draw reliable conclusions, are not represented.) Cross, messy erratic: high values of both coordinates. Neuron with a natural rate of 7.84 s^{-1} was driven at a rate of 3.77 s^{-1} (ratio 0.48); the resulting postsynaptic rate was 6.54 s^{-1}. Same form, but not the same trains as in Figs 8, 11 (some epochs) and Plate E of Ref. 51. Star, stammering: intermediate nonlinearity and negligible slope. Neuron with a natural rate of 14.4 s^{-1} was driven at a rate of 18.2 s^{-1} (ratio 1.26); the resulting postsynaptic rate was 6.41 s^{-1}. Adapted from, and including the same train as, Fig. 9 and Plate F in Ref. 51.

or, as the train represented (black circle), the erratic forms.

4. DISCUSSION

The present analyses of spike train forms from prototypical living neurons, based essentially on different aspects of their predictabilities, led to conclusions that concerned their dimensionality, nonlinearity and the rate of decay of prediction success with time (i.e. forecast horizon). In this fashion, it became possible to move past the conventional view that predictability must always correspond to simplicity and likewise complexity to unpredictability. Nonlinear analytical techniques demonstrated a range of behaviors differing in terms of dimensionality, linearity and the potential presence of chaotic dynamics. This strengthens a classification of spike trains into separate forms advanced earlier[51] that had, in turn, gone beyond the less informative grouping into locked (periodic, regular) and not-locked (aperiodic, irregular) trains.[29,42,48]

Results also demonstrated the identity of these forms with universal behaviors known to nonlinear dynamics:

(1) Lockings are periodic behaviors that admit linear models.[5,29,30,42,48,49,60,70] Hayashi's synaptically driven ''1:1 entrainment'' is a 1:1 locking.[24] Some earlier findings suggested that relatively simple, even linear models would suffice for periodic locked trains (and for their coding from presynaptic pacemaker trains).[5,29,30,42,48,49,60,70] For example, plots of interval lengthening as a function of inhibitory postsynaptic potential (IPSP) phase are linear, as is the relation between corresponding averages within each *p:q* locking domain (say, a slope 1 line for 1:1 lockings). The present study confirms linearity for 1:1 lockings; we conjecture that linearity will be generalized to all ratios. Other earlier findings showed some complexities, as, for example, a piecewise linear with slopes 1, 1/2, 2,..., i.e. nonlinear, overall relation between averages: hence, even if linearity exists for each locking, its slopes and intercepts probably change from one to the next.

(2) Poisson-driven trains are strongly irregular behaviors best forecast by nonlinear models. Prediction errors, much smaller for lockings than for Poisson drivings, where they mainly reflect arrival irregularity, are invariant with time for both (i.e. forecast horizons are long). Therefore, the part of the signal not forecast successfully is indistinguishable from uncorrelated, additive noise.

(3) Intermittent trains require nonlinear models. Analytic models suggest that such data sets arise close to points where small changes in control parameters destabilize limit cycles (see below).[3,35,36] In fact, intermittencies arise close to periodic and chaotic behaviors, presumably at transitions between them. What follows summarizes the main notions about intermittency, as set forth in significant contributions by Bergé and collaborators.[3,4] Intermittency, they point out, is an essentially qualitative concept that applies when data sets, called ''intermittent'', appear regular most of the time, but destabilize briefly in variable bursts that arise irregularly. Such sets are not uncommon and, whereas conventional statistics are not too helpful, the

concept of intermittency has contributed markedly to their experimental and formal analysis. The regular portions impose the prevalent periodicities; irregularities within the bursts and in the interburst intervals impose other periodicities. The overall spectrum may either: (i) have strong peaks at frequencies not related linearly with rational coefficients, (ii) have weak peaks plus strong background noise or (iii) be somewhere in between. Such spectra mean that the intermittency's irregularities can impose, respectively, quasiperiodic, chaotic or intermediate characteristics. The notion of intermittency thus overlaps partially with those of quasiperiodicity and chaos, and intermittent data sets may be also quasiperiodic or chaotic. Accordingly, certain questions can be answered only generally, clarifying extreme cases but leaving intermediate ones uncertain. For example, the answer to whether a train that behaves intermittently and has chaotic components should be called ''intermittent'' or ''erratic'' depends on which feature is prevalent: Fig. 2iii represents a train labelled ''intermittent'' because its intermittent character is outstanding and, though also hard to describe and summarize, its chaotic nature is convincing only after tests show non-invertible interval and phase return maps, low dimensionality, nonlinearity, and short prediction horizons and thus significant deterministic chaotic dynamics. Prevalence is not always obvious, however.

(4) Phase walk throughs, discovered in interacting fireflies, are intermittencies where the regular portions are relatively brief, and the phases cross their range repeatedly along slightly different paths.[12] Their return maps are invertible: the interval maps (Fig. 4iv), apparently non-invertible, become invertible with special polar coordinates;[38] the phase maps are obviously invertible.[51] Formally (see below), phase walk throughs are explained by one-dimensional map iterations, and represented well by quasiperiodicities, i.e. mixtures of periodic variables that are irrational multiples.[3,4] A salient feature of experimental walk throughs is that only brief stationary portions arise experimentally.[52] This can be due to attractor basins only slightly broader than the volume swept by the unavoidable noise; it is compatible with the hypothesis that walk throughs arise only with driver rates very close to those for lockings[12] (and, as noted, their brevity hinders nonlinear analyses).

(5) Erratic spike trains have short horizons, non-invertible maps, and are maximally nonlinear[51]; their messiness reflects chaotic trajectories. Synaptically driven spike trains (*Onchidium*) with heterogeneous intervals and non-invertible maps are probably chaotic.[24]

(6) Messy stammerings have long horizons and are marginal between linear and nonlinear; their messiness is noise-related. Modeling studies of cold receptors by Longtin and Hinzer[32] are particularly relevant to the relative contributions of deterministic issues and the inevitable noise: contrasting models—one with noise and without chaos, the other with chaos and without noise—are valid across broad temperature ranges and, possibly depending on the temperature, one or the other may be preferable and one issue or the other preponderant. Chaos may exists in crayfish too, but occupy a volume smaller than that swept by noise.[60]

As argued elsewhere,[54,58] the facts that pacemaker-driven forms (i, iii–vi) are imposed by the simplest pattern of all and persist when pacemaker patterns are perturbed by irregularities, trends or periodic modulations, suggest such forms are elementary building blocks for many synaptic codings. Their robustness notwithstanding, sufficiently large presynaptic departures away from pacemakers modify and even eliminate such basic forms.[29,54,58] Hence, one should ask if, for the present pacemaker-based considerations to hold, trains must be strictly pacemaker or whether restrictions about, say, lack of trends can be relaxed. If relaxations are tolerated, one should also ask by how much, i.e. which are the respective domains, and related questions such as the trains that arise in each. This means applying procedures such as those described here to trains driven by, for instance, irregular, transient or modulated inhibition.[29,54,58] Finally, it is necessary to ask specifically if the biological implications of the present work are restricted to SAO-like cases, or extend to broader classes of neurons and synapses: we suggest that they do apply broadly in qualitative terms.

4.1. *Formal models and system partition*

Naturally functioning neurons are complicated systems involving numerous physical variables that, at cellular, subcellular and other levels, imply transmitter release, conductances, pumps, neuronal inhomogeneity, PSPs, action potentials, etc.:[11,29,48,50] conceptual representations based on that many variables are bound to be unmanageable. As operational entities, however, neurons are mimicked satisfactorily by models involving formal variables in smaller numbers (see Section 4.2.). The success of these compacted models suggests that the system is dissipative, operationally exhibiting fewer degrees of freedom than would be suspected from even incomplete lists of physical variables.

It is as if operational compacting meant that: (i) the physical variables coalesced into separate groups or subsystems, (ii) the component variables within each subsystem cooperated and emerged as a single parameter, and (iii) ultimately, the dynamic interactions of those subsystems determined the overall

behaviors that the formal model in question describes. A suggestive example is FitzHugh's streamlining of the Hodgkin–Huxley (HH) formulation.[13] In short, the system is *de facto* partitioned into subsystems whose dynamics generate the global dynamics: each partition is identified by its particular set of subsystems, its particular dynamics, or both.

Experiments demonstrate that each presynaptic timing—average, pattern—imposes a characteristic form. This implies that each timing imposes a characteristic partition, making the physical variables coalesce into particular subsystems with particular interactions. The number of such subsystems, unknown beforehand, was determined from the data by estimating for each form its number of dimensions (operational variables, degrees of freedom, active modes), i.e. the dimensionality of the attractor on which the system moves (see Results). Experiments demonstrate also that different timings impose different forms, i.e. partitions that differ in component subsystems and/or dynamics.

This partitioning into interacting subsystems and its dependence on the presynaptic timing are, we feel, major points. They are relevant whenever systems are forced into different behaviors by different drives, and thus raise issues of general interest. The following considerations are pertinent, though largely conjectural. The number of partitions that differ exclusively because their component subsystems differ (irrespective of dynamics) should be high. Indeed, estimates of upper bounds must be high, initially at least, since they must take into account: (i) a usually high number of physical variables, (ii) an even higher number of subsystems these variables could coalesce into, and (iii) the many ways in which, from that set of subsystems, one could pick D of them, D being the number of dimensions. For example, if the system has 10 physical variables (a parsimonious guess) and $D=4$, there are roughly up to 1000 subsystems and 2^{35} partitions (exactly, 2^{10} and $[2^{10}(2^{10}-1)(2^{10}-2)(2^{10}-3)]/4!$, respectively). Physical constraints must substantially reduce the number of possible partitions that differ because of the subsystems that compose; it is likely, however, that this number remains considerable.

Partitions may also differ by dynamics that, involving the variables and subsystems, manifest themselves in vast arrays of functionally meaningful measurements and criteria. A particularly important feature introduced by the dynamics is that these manifestations and criteria are often continuous. Hence, the set of partitions that differ only because of component subsystems, discrete and with a countable number of them, is expanded to a continuous set with subsystems in uncountable numbers.

Conjectures 1–4 are compatible with data; for simplicity, they concentrate on particular forms within single, undivided domains and imposed by different pacemaker averages (e.g., on only 1:1 and not all *p:q* lockings).

Conjecture 1. A particular form involves in all points of its domain practically the same subsystems; only their dynamics change. When averages move from one value to another within the domain, changes involve at most few and uninfluential variables; the dynamics change significantly, but only quantitatively, remaining qualitatively invariant. For instance, all 1:1 lockings (arising with averages around the natural value) involve the same subsystems; the trajectories of variables relating to the SAO's phase remain limit cycles, only changing periods. Hence, the partition set is practically uniform and continuous within each domain.

Conjecture 2. Different forms involve significantly different subsystems and dynamics. When averages cross to a different domain, at least some subsystems differ in influential variables, and the dynamics change qualitatively. For example, 1:1 lockings and intermittent forms in nearby domains share some but not all subsystems; moreover, the trajectory dynamics of the variables change qualitatively. The partition set changes abruptly, dramatically perhaps, at the domain's boundaries.

Conjecture 3. These conjectures can be extended to perturbations.[29,30,54,58] When, say, the presynaptic interval is modulated periodically, increasing and decreasing monotonically in a repeated manner,[58] partitions change unceasingly: within the domain of a particular form they involve mainly the dynamics but, when crossing to another domain, both partitions and dynamics change.

Conjecture 4. This notion of driver-induced partitions suggests a strategy for clarifying the relation between physical and formal variables, i.e. recognizing the physical variables in each subsystem and thus the roles played by these variables in the different forms. The strategy is based on the parallel driving of a formal model and one with explicit physical variables (say, the Bonhoeffer–van der Pol and that of Edman and collaborators, respectively[11,35]), and comparing identical forms. It is likely that in each form the physical variables within each subsystem will all behave in a special way that resembles that of the corresponding formal variable and, in addition, have closer and/or simpler correlations.

4.2. *Data and their formal analyses*

Data from living preparations reveals an assortment of complexities, regularities and predictabilities, and our understanding or them has benefitted from appeals to formal models. The following summarizes a strategy applicable to all periodic operations affected by brief periodic perturbations, regardless of physical embodiment. It was introduced by Glass and collaborators[14,16–19,21,22,41] who implemented it successfully when forcing cardiac cell aggregates (alluded to here as ''heart cells'') from chick embryos with outward current pulses. Because IPSPs reflect

brief synaptic changes, the strategy is applicable to periodically inhibited SAO pacemaker neurons. The following also summarizes both implementations with heart cells and SAOs, whose similarities and differences, spanning from elementary curves to overall behaviors are, we feel, instructive.

The approach involves certain assumptions and follows several stages. Assumptions 1–4 are initially accepted:

Assumption 1. The system is invariant along time, and noiseless; its model has an attractive limit cycle that imposes a natural period (interval) and an unstable steady state.

Assumption 2. Perturbations (stimuli) are brief, equal and periodic.

Assumption 3. The consequences of each perturbation last less than the oscillator's natural interval and the inter-perturbation interval.

Assumption 4. Characteristic functions, called ''phase transition curves'' (PTCs) express one phase as a function of the preceding one [by, say, one-dimensional nonlinear equations $x_k = f(x_{k-1})$]; ''phase'' means the perturbation's position relative to the driven oscillator's cycle.

Because of Assumptions 1–4, PTCs map the unit circle into itself.[17] PTCs change with the perturbation's amplitude. Implementation follows stages 1–5:

(1) By delivering to the preparation sporadic stimuli, an [interval, phase] plot of perturbed interval as a function of phase (both normalized to natural periods) is obtained for each pulse amplitude. ''Sporadic'' means at irregular intervals, all longer than several times the natural period. Plots differ by constants from [lengthening, phase] or ''delay functions''.
(2) An analytic expression is found that, by simply changing parameter values, fits the [interval, phase] plot at all stimulus amplitudes.
(3) Under the assumptions listed, the perturbed interval's duration equals the sum of the natural period plus the extant phase and minus the following phase. The perturbed interval and the following phase can be expressed as functions of the extant phase by, respectively, the [interval, phase] plot and the PTC. Hence, PTCs can then be determined from the available phases and natural period.
(4) A model based on iteration of the PTC one-dimensional map, i.e. by obtaining each phase (the second, third, etc.) from the preceding one, is tested.[17] Adjusted for stimulus amplitude and period, it simulates periodic driving and generates certain timings and forms. The experimental data and these theoretical results are compared, coincidences and discrepancies are identified, and judgments are made as to the model's suitability (see below).
(5) Other models (i.e. maps and differential equations) are tested by running simulations, involving periodic driving and generation of timings and forms. Though parsimony is a virtue in any model and simple models can have interesting behaviors,[19,41,46] complex findings often require higher dimensional plots and more elaborate models. Model parameters are either mainly theoretical or represent recognized physical variables as in, say, the BVP or HH cases. The BVP is a system of differential equations that, properly adjusted, has an asymptotically stable limit cycle and an unstable equilibrium point. Its variables represent membrane potential, refractoriness and stimulating currents, one invariant, another a pulse sequence. Separate cycle regions have slow and fast dynamics, a feature that makes it a good neuronal model (as it does the modified radial isochron clock):[35–37] it is, in fact, a simplified version of the HH equations.

Comparisons between experiments and theory are achieved by placing the relatively sparse set of experimental results upon the broader background of detailed theoretical bifurcation diagrams and noting coincidences and discrepancies:[22] amplitude and period are the control parameters. Coincidences and discrepancies always exist, and models are evaluated by balancing them. Coincidences, obviously, are assets; so are discrepancies insofar as, when identifying what went wrong, they provide insights about unexpected aspects of the dynamics and therefore suggest useful adjustments.

The more a model's assumptions comply with the reality of a particular embodiment, the more successful its use will be. An assumption is acceptable either because it is close to reality or because it provides an opportunity for simplification, the essence of modeling. As noted by Glass *et al.*,[17] assumptions about the absence of noise and long-term effects (1, 3) though initially acceptable, must be applied with particular caution: heart cells and SAOs differ somewhat in this respect.

After-effects can appear following single perturbations, increase with more and extend beyond their cessation. Usually negligible when intervals between arrivals are long, they may change the system's properties and become influential when short. Noise is unavoidable (so are measurement errors, negligible here);[15,16,57] it displaces boundaries, modifies, introduces or eliminates forms and, in regions with several neighboring basins, induces jumps between them (''hoppings''[51]). As explained above, the significance of noise and after-effects is recognized and evaluated by data-based estimates of dimensionality and predictability, e.g., embeddings and prediction times. Precise demonstration of certain roles for after-effects or noise and their details may require specialized projects generally not yet attempted. (The stationarity assumption may be violated too, if trains include the initial transients: this did not happen in heart cells or SAOs.)

4.2.1. *Heart cells*. Implementation in heart cells driven by excitatory outward current pulses, used as a blueprint, showed the following.[14,16–19,21,22,41]

(1) Experimental [interval, phase] plots were (roughly) piecewise linear, increasing to a maximum, then decreasing to a minimum, and finally increasing. The shortest or longest phases caused, respectively, interval lengthenings or shortenings. Greater amplitudes increased maxima, decreased minima and made slopes steeper.

(2) These plots and their amplitude dependence were fitted well by analytic functions with sums of exponentials.

(3) As pulse amplitudes increased, PTCs (derived from those functions) changed from monotonic to non-monotonic and from invertible to non-invertible. At the largest amplitudes, points tended to disappear from the decreasing portion that became practically discontinuous, and the analytic functions did not hold.

(4) Iterations of those nonlinear one-dimensional PTCs had the following outcomes: (i) at amplitudes where maps were monotonic, bifurcation diagrams were simple showing lockings with rational *p:q* ratios in regions called ''Arnol'd tongues'' and quasi-periodicities with irrational ratios (intermittencies) between those tongues. Forms were independent of the initial conditions. Only tangent bifurcations occurred: in ''tangent bifurcations'', PTCs successively intersect, become tangent to and separate from the diagonal. (ii) Where PTCs were non-monotonic, the bifurcation diagram structure was complex and, less thoroughly understood, needs further analysis (e.g., two-dimensional maps). Arnol'd tongues with different lockings overlapped: for a fixed amplitude, different periods could impose stable cycles at the same ratio but still dissimilar (e.g., *p:q*, 2*p*:2*q*); for fixed amplitude and period, bistability occurred. ''Bistability'' means that, depending on the initial conditions, different ratios or forms appear. Substantial areas included aperiodic forms sensitive to initial conditions. At the outer boundaries of Arnol'd tongues, tangent bifurcations separated lockings and quasiperiodicities but, at their inner boundaries, periods switched from *q* to 2*q* in cascades (*q*, 2*q*, 4*q*, etc.), i.e. period-doubling bifurcations were present. Yet other bifurcations arose, but not all can be formally identified or interpreted, at least exclusively with one-dimensional maps. The existence of deterministic chaos is supported by the non-monotonic PTCs, by demonstrable bistability (sensitivity to initial conditions), as well as by the presence of accepted routes such as tangent or period-doubling bifurcations.

Consequently, the system is well described by one-dimensional resetting curves: these, obtained from single stimuli and iterated, allowed accurate theoretical predictions of the different dynamic rhythms experimentally observed, as well as their orderings and overall organizations. Discrepancies were significant when arrival intervals were briefer than natural intervals, and are attributable to after-effects.[16] These cases would benefit from analysis of maps of two or more dimensions and other models (stage 5). Recognized after-effects are, say, that cessation of prolonged stimulation at long or short intervals is followed by, respectively, heart cell acceleration (''underdrive acceleration'') or slowing (''overdrive suppression'').[16] Discrepancies attributable to noise, less important, were that the model's boundaries of 1:1 locking regions corresponding to the shortest intervals differed from those in heart cells in some locations and had more heterogeneous neighborhoods (e.g., with 7:6 locking or aperiodic forms). On the balance, then, the model based on one-dimensional nonlinear map iteration is highly satisfactory.[9,14,16–19,21,22,41] Its dynamics agree closely over broad domains with experimental heart cell dynamics and, in addition, extend to the normal and abnormal whole heart.

(5) The BVP model is comparably successful to PTC iterations, but less simple.[22] Conceivably it can contribute additional insights when, because the consequences of each arrival exceed natural or inter-perturbation intervals, Assumption 3 is violated [see Section 4.2.2 (5)]. HH models (more or less modified) include the ionic mechanisms:[9,19] those underlying phase resettings by current pulses are complex, depending upon polarities, amplitudes and phases but their dissection by Clay and collaborators[9] provide frameworks for topological analyses of periodic drivings. The Poincaré maps of such models account for several observed behaviors.[22]

4.2.2. *Slowly adapting stretch receptor organ or postsynaptic neuron*[5,29,30,42,48,49,53,60,70]. (1) Experimental [interval, phase] plots obtained with sporadic IPSPs showed that periods increased with phases.[5,29,42,48] Only presynaptic periods were examined parametrically, however, because all preparations had similar IPSPs, i.e. amplitudes. (2) Best fits were straight lines with slopes around 0.7. (3) PTCs obtained from those plots were monotonic and invertible. (4) Their simulated iterations (as did other models such as leaky integrators), examining both periods and amplitudes, led exclusively to *p:q* lockings and quasiperiodicities located, respectively, within Arnol'd tongues and between them; forms were separated by tangent bifurcations and were independent of the initial conditions.[30,42,48,49,60,70,71] Extensive simulations did not show other forms or bifurcations which, therefore, were either not generated or present only in hard-to-find domains.

Thus, the agreement between the dynamics of iterated one-dimensional maps with those exhibited by the SAO[29,42,48,51,52] was restricted to the simpler, more regular and predictable forms and bifurcations: this identifies what suffices for the simpler forms. Significant discrepancies existed, however, such as the lacks of chaotic intermittencies, messy forms

(erratic, stammering) and of other bifurcations: it seems, therefore, that iteration models need complementing [see (5) below].

One can reasonably assign a major role in these discrepancies to nonlinear after-effects and to noise. Noise is discussed in (5) below. Well-demonstrated after-effects are powerful, long-lasting and depend on IPSP and postsynaptic timings.[29,48,51,52,54] Firstly, [interval, phase] plots for sporadic IPSPs can be piecewise linear (increasing–decreasing), for IPSP pairs can be multivalued,[29] and for current or sensory pulses resemble those in heart cells (Diez Martínez, unpublished observations).[5,29,52] Moreover, IPSPs also modify the next interval (shortening or lengthening it), and this increases with more arrivals.[29,48,52] Finally, SAOs escape the silencing influence of high-rate IPSPs.[29,51] After-effects thus change the system, negligibly with sporadic IPSPs, but strongly and significantly as inter-arrival intervals shorten, approaching and then becoming shorter than natural ones. Such effects, we believe, contribute to the complexities such as messy erratic (chaotic) and stammering trains.

(5) Accordingly, the situation was simulated using primarily BVP models, and secondarily others.[35–37,60,61] Phases in simulations were still IPSP positions in postsynaptic cycles (identified in special ways) but, in crayfish, were postsynaptic spike positions in inhibitory cycles. Finally, return maps, including the same or more dimensions, were based on the ongoing trains themselves, and not on sporadic stimuli (Fig. 5).

Numerical computation of driven BVP models showed complex [amplitude, period] bifurcation diagrams, whose features reflected the geometries of the limit cycles, equilibrium points, nullclines and perturbations.[35,36] A ''nullcline'' is formed by the points where a particular state variable does not change, i.e. has zero derivative. Regions with characteristic forms and PTCs revealed domains wherein the system can be described properly by iterated one-dimensional PTCs, and others where it cannot.

Certain regions in the [amplitude, period] diagram are noteworthy. Region 1: weak amplitudes, any period. PTCs were monotonic, invertible and, more or less close to the diagonal, and adequately describe the dynamics. Quasiperiodic responses predominated, coinciding with the nonchaotic intermittencies called phase walk throughs; locked responses were hard to find. Region 2: intermediate amplitudes, periods around natural intervals. PTCs were non-monotonic and non-invertible, and their overall shape varied little over most of the phases; at the larger end, however, PTCs were very steep and small old phase changes generated remarkably different new phases. Within this region, the following happened, as periods I increased: (i) PTCs intersected the diagonal at one stable point, and 1:1 locking was present. (ii) PTCs became tangent and then separated from the diagonal; trains became intermittent and chaotic. (iii) PTCs intersected the diagonal twice, creating two stable points; which was achieved depended on the initial conditions. (iv) Only one stable point subsisted (period 1), then destabilized, was substituted by stable points of, successively, periods 2, 4 or longer, and eventually erratic trains; bistability was present. Region 3: intermediate amplitudes, periods shorter than natural intervals. As Is changed, first a 3:1 locking existed; then PTCs became tangent to the diagonal, and finally separated from it. Chaotic stammering arose: postsynaptic intervals belonged to categories that differed approximately by a fixed amount; their return maps were lattices with several clusters, and the between-cluster sequence was difficult to predict.

Compatibility between the SAO and the BVP models was close,[29,42,48,51,52] involving first forms and bifurcations. Furthermore, SAO data coincided closely with the subset of the BVP diagram extending throughout the period scale within an intermediate amplitude band. Discrepancies, major or minor, were few. In the SAO, domains were largest for 1:1 lockings, all locked and all chaotic forms were about equally frequent and no $2p$:$2q$ separate from p:q lockings occurred. In the BVP, domains were largest for 2:1 lockings, locked forms prevailed and $2p$:$2q$ lockings occurred. Moreover, whereas for stammerings in SAOs intervals differed by multiples of I, clusters lacked recognizable structure, and phases were extreme (i.e. 0, 1), in the BVP differences were not multiples of I, clusters had intrinsic structures, and phases were not always extreme. Hoppings, i.e. unpredictable shifts between forms during stationary driving, present in SAOs are absent in the BVP, as in all noise-free models.[51]

Discrepancies can be attributed tentatively first to nonlinear after-effects [see Section 2.2.2 (4)]. Noise[32,51,57,60] generally participates by reducing or abolishing the smaller domains (e.g., 5:6 and $2p$:$2q$ locked) and thus simplifying. By irregularizing forms, it makes them seem messy and thus misleads into overestimating their proportions; in stammerings, by occupying a volume greater than deterministic variability, it washes out the clusters' internal structure; in hoppings, it switches between nearby forms. Theoretically, noise implies infinite dimensions and embedding is of little use; practically, however, fewer may suffice for models that, though not exhaustive, are acceptable. The noisy character of nonlinear Poisson-driven forms is imposed by the input.

Thus, BVP equations represent quite fully the driven SAO's dynamical system, and tell us a great deal about it: they are, therefore, useful tools for subsequent analyses including, say, those of transient and modulated drivings.[54,58] In particular, the BVP model also opens the door for achieving deterministic interpretations of stammerings (i.e. messy forms driven at short intervals), so far lacking. Nomura *et al.*[35] outline a qualitative explanation based on the

fact that tightly packed arrivals when the system point is close to the unstable equilibrium point can have contrasting consequences, one followed almost immediately by a spike, another by a slow displacement around the unstable point without spiking.

The ''permeability model'' of Edman *et al*., analysed by Stiber, includes identified permeabilities, ionic fluxes, and so forth.[11,60,62] Though incompletely examined, it duplicates SAO behaviors faithfully: a significant discrepancy is the internal structure of clusters in stammerings. The slower variables are necessary for after-effects and complex forms (Stiber, unpublished observations).

As demonstrated, theoretical computations can successfully explain and predict rhythms observed experimentally and their orderings, identify possible sources of discrepancies, guide experimental designs and ultimately provide significant insights. Noted also is that caution is mandatory when relating natural phenomena and formalizations and thus meshing different disciplines, such as biology and mathematics.[14,19,45] Indeed, stumbling blocks can reflect, for example, undeveloped concepts, strategies and procedures, contrasts between rigorous demonstrations using models with less certain ones using data and, possibly, some unawareness and misunderstanding between specialists in disparate fields.

5. CONCLUSIONS

The methods used here (and comparable ones) are applicable to any spike train described by its ordered set of intervals, regardless of whether driven synaptically.[8,23,28,31–33,43,63,63–67,73] Their usefulness is reinforced because often in the neurosciences one only has access to the spike trains of individual neurons, and these methods provide the experimental foothold for formal constructs.

A commonplace and justified conception of the nervous system is a network composed of spike-generating, synaptically connected neurons wherein spike trains are major signs of ongoing input, output or intrinsic transactions. The spike-generating neuron and its synaptic constellation provide the operational unit for nervous systems so conceived, as well as for entities designed to mimic them. The crayfish stretch receptor preparation is a prototype for a particular kind of inhibitory connection, and principles inferred from its analyses are applied broadly. Such generalizations include the synaptic arrangement composed of sets of numerous weak convergent terminals, so prevalent within nervous systems.[56,57] Indeed, as the individually weak terminals become more correlated, i.e. fire more synchronously, those sets tends to perform like single powerful terminals, and therefore to elicit the same forms. The degree of correlation is modulated unceasingly during natural operation.

Because biology rightly assigns significance to regularity, to irregularity, and to contrasts, gradations, transitions and alternations among them, analyses of dimension, nonlinearity and forecasting are meaningful, not just formally but also biologically. Their controls by single neurons or circuits have been explored well for periodic functions, but little (except as weakenings of periodicity) for aperiodic functions whose full meanings are only beginning to be understood.[1,2,19,56,72] Command neurons can be irregular, either spontaneously or forced by intercurrent, e.g., synaptic, perturbations and, as demonstrated, can impose a variety of post-synaptic timings by changing their averages and/or patterns. Present results show how command neurons, manipulating only a few parameters in their spike trains, can subtly control irregularity, complexity and unpredictability.

For example, chaotic irregularity is known to include several neighboring unstable periodic orbits and be specifically sensitive to small perturbations.[39] Consequently, appropriate perturbations can maintain a desired periodicity, or switch between different ones. This general notion applied to spike trains means that chaotic ones (e.g., erratic) have several unstable preferred intervals and that small driver changes could specifically stabilize or switch to some other. It is likely that such dynamic behaviors have important roles in many vital functions, particularly those involving regular and irregular behaviors.

Acknowledgements—Supported by the Hong Kong Research Grants Council (HKUST 187/93E, 527/94M, 668/95E) (MS) and Trent H. Wells Jr, Inc. (JPS).

REFERENCES

1. Aihara K. (1994) Chaos in neural response and dynamical neural network models: towards a new generation of analog computing. In *Towards the Harnessing of Chaos* (ed. Yamaguti M.), pp. 83–98. Elsevier, Amsterdam.
2. Aihara K. (1995) Chaos in axons. In *The Handbook of Brain Theory and Neural Networks* (ed. Arbib M.), pp. 183–185. MIT Press, Cambridge, MA.
3. Bergé P. and Dubois M. (1988) Etude expérimentale de l'intéermittence et le chaos en convection de Rayleigh-Bénard. In *Le Chaos. Théorie et Expériences* (ed. Bergé P.), pp. 1–83. Eyrolles, Paris.
4. Bergé P., Pomeau Y. and Vidal C. (1984) *L'Ordre dans le Chaos.* Hermann, Paris.
5. Buño W., Fuentes J. and Barrios L. (1987) Modulation of pacemaker activity by IPSP and brief length perturbations in the crayfish stretch receptor. *J. Neurophysiol.* **57,** 819–834.
6. Casdagli M. (1989) Nonlinear prediction of chaotic time series. *Physica D* **35,** 335–356.
7. Casdagli M. (1992) Chaos and deterministic versus stochastic modelling. *J. Roy. statist. Soc. B.* **54,** 303–328.

8. Chillemi S., Barbi S. and Di Garbo A. (1997) Dynamics of the neural discharge in snail neurons. *Biosystems* **40,** 21–28.
9. Clay J., Guevara M. and Shrier A. (1984) Phase resetting of the rhythmic activity of embryonic heart cell aggregates. *Biophys. J.* **45,** 699–714.
10. Diez Martínez O., Pérez R., Budelli R. and Segundo J. P. (1988) Locking, intermittency and bifurcations in regularly driven pacemaker neurons. Poincare mappings and biological implications. *Biol. Cybern.* **60,** 49–58.
11. Edman Å., Gestrelius S. and Grampp W. (1987) Analysis of gated membrane currents and mechanisms of firing control in the rapidly adapting lobster stretch receptor neurone. *J. Physiol., Lond.* **384,** 649–669.
12. Errmentrout G. and Rinzel J. (1984) Beyond a pacemaker's entrainment limit: phase walk-through. *Am. J. Physiol. (Reg. integ. comp. Physiol.)* **246,** R102–R106.
13. FitzHugh R. (1961) Impulses and physiological states in theoretical models of nerve membrane. *Biophys. J.* **1,** 445–466.
14. Glass L. (1995) Chaos in neural systems. In *The Handbook of Brain Theory and Neural Networks* (ed. Arbib M.), pp. 186–189. MIT Press, Cambridge, MA.
15. Glass L., Graves C., Petrillo G. and Mackey M. (1980) Unstable dynamics of a periodically driven oscillator in the presence of noise. *J. theoret. Biol.* **86,** 455–475.
16. Glass L., Guevara R., Belair J. and Shrier A. (1984) Global bifurcations of a periodically forced biological oscillator. *Phys. Rev. A* **29,** 1348–1357.
17. Glass L., Guevara R., Shrier A. and Pérez R. (1983) Bifurcation and chaos in a periodically stimulated cardiac oscillator. *Physica D* **7,** 89–101.
18. Glass L., Kaplan D. and Lewis J. (1992) Tests for deterministic dynamics in real and model neural networks. In *Proceedings of the Second Annual Conference on Nonlinear Dynamical Analysis of the EEG* (eds. Jansen G. and Brandt M.), pp. 233–249. World Scientific, Singapore.
19. Glass L. and Mackey M. (1988) *From Clocks to Chaos.* Princeton University Press, Princeton.
20. Glass L. and Pérez R. (1982) Fine structure of phase locking. *Phys. Rev. Lett.* **48,** 1772–1775.
21. Glass L., Shrier A. and Bélair J. (1986) Chaotic cardiac rhythms. In *Chaos* (ed. Holden A.), pp. 236–256. Princeton University Press, Princeton.
22. Guevara M., Glass L., Mackey M. and Shrier A. (1983) Chaos in neurobiology. *IEEE Trans. Syst. man. Cybern.* **13,** 790–798.
23. Hastings H. and Sugihara G. (1995) *Fractals. A User's Guide for the Natural Sciences*. Oxford University Press, New York.
24. Hayashi H. (1993) Chaos in biological, neural systems. In *Proc. Joint Technical Conf. Circuits/Systems, Computers and Communications*, Vol. 1, pp. 282–285. Nara, Japan.
25. Hayashi H. and Ishizuka S. (1995) Chaotic responses of the hippocampal CA3 region to a mossy fiber stimulation *in vitro*. *Brain Res.* **686,** 194–206.
26. Hayashi H., Ishizuka S. and Hirakawa K. (1985) Chaotic response of the pacemaker neuron. *J. Physiol. Soc. Japan* **54,** 2337–2346.
27. Ishizuka S. and Hayashi H. (1996) Chaotic and phase-locked responses of the somatosensory cortex to a periodic medial lemniscus stimulation in the anesthetized rat. *Brain Res.* **723,** 46–60.
28. Kaplan D. and Glass L. (1992) Direct test for determinism in a time series. *Phys. Rev. Lett.* **68,** 427–430.
29. Kohn A., Freitas da Rocha A. and Segundo J. (1981) Presynaptic irregularity and pacemaker inhibition. *Biol. Cybern.* **41,** 5–18.
30. Kohn A. and Segundo J. (1983) Neuromime and computer simulations of synaptic interactions between pacemakers. Mathematical expansions of existing models. *J. theoret. Neurobiol.* **2,** 101–125.
31. Longtin A. (1993) Nonlinear forecasting of spike trains from sensory neurons. *Int. J. Bifurc. Chaos* **3,** 651–661.
32. Longtin A. and Hinzer K. (1996) Encoding with bursting, subthreshold oscillations and noise in mammalian cold receptors. *Neural Comput.* **8,** 215–255.
33. Moss F. (1995) The crayfish caudal photoreceptor: a forced nonlinear oscillator with low dimensional deterministic behavior. In *Proceedings of the International Workshop on Neuronal Coding*, p. 38. Prague, Czech Republic.
34. Mpitsos G., Burton R., Creech H. and Soinilla S. (1988) Evidence for chaos in spike trains of neurons that generate rhythmic motor patterns. *Brain Res. Bull.* **21,** 529–538.
35. Nomura T., Sato S., Doi S., Segundo J. and Stiber M. (1994) A Bonhoeffer–van der Pol oscillator model of locked and non-locked behaviors of living pacemaker neurons. *Biol. Cybern.* **69,** 429–437.
36. Nomura T., Sato S., Doi S., Segundo J. and Stiber M. (1994) Global bifurcation structure of a Bonhoeffer–van der Pol oscillator driven by periodic pulse trains. Comparison with data from a periodically inhibited biological pacemaker. *Biol. Cybern.* **72,** 55–67.
37. Nomura T., Sato S., Doi S., Segundo J. and Stiber M. (1994) A modified radial isochron clock with slow and fast dynamics as a model of pacemaker neurons. Global bifurcation structure when driven by periodic pulse trains. *Biol. Cybern.* **72,** 93–101.
38. Ott E. (1993) *Chaos in Dynamical Systems*. Cambridge University Press, Cambridge.
39. Ott E., Gregogi C. and Yorke J. (1990) Controlling chaos. *Phys. Rev. Lett.* **64,** 1196–1199.
40. Zimmermann P. E. R. I, Vining E., Cohen N., Albano A. and Jiminez Montano M. (1994) The algorithmic complexity of neural spike trains increases during focal seizures. *Neuroscience* **14,** 4731–4739.
41. Pérez R. and Glass L. (1982) Bistability, period doubling bifurcations and chaos in a periodically forced oscillator. *Phys. Lett. A* **90,** 441–443.
42. Perkel D., Schulman J., Bullock T., Moore G. and Segundo J. (1964) Pacemaker neurons: effects of regularly spaced synaptic input. *Science* **145,** 61–63.
43. Racicot D. and Longtin A. (1995) Reconstructing dynamics from neural spike trains. In *Proceedings of the 17th IEEE Conference in Medicine and Biology*, 20–23 September, Montréal, Canada, Vol. 2, pp. 1477–1478. .
44. Rapp P., Zimmermann I., Albano A. and Greenbaun N. (1985) Dynamics of spontaneous neural activity in the simian motor cortex: the dimension of chaotic neurons. *Phys. Lett.* **110A,** 335–338.
45. Ruelle D. (1989) *Elements of Differentiable Dynamics and Bifurcation Theory*. Academic, New York.

46. Sato S. and Doi S. (1992) Response characteristics of the BVP neuron model to periodic stimuli. *Math. Biosci.* **112,** 243–259.
47. Schaffer W. and Kot M. (1985) Do strange attractors govern ecological systems? *BioScience* **35,** 342–350.
48. Schulman J. (1966) *Information Transfer Across an Inhibitor to Pacemaker Synapse at the Crayfish Stretch Receptor*. Ph.D. thesis, University of California, Los Angeles.
49. Segundo J. (1979) Pacemaker synaptic interactions: modelled locking and paradoxical features. *Biol. Cybern.* **35,** 55–62.
50. Segundo J. (1986) What can neurons do to serve as integrating devices? *J. theoret. Biol.* **5,** 1–59.
51. Segundo J., Altshuler E., Stiber M. and Garfinkel A. (1991) Periodic inhibition of living pacemaker neurons. I. Locked, intermittent, messy and hopping behaviors. *Int. J. Bifurc. Chaos* **1,** 549–581.
52. Segundo J., Altshuler E., Stiber M. and Garfinkel A. (1991) Periodic inhibition of living pacemaker neurons. II. Influences of driver rates and transients and of non-driven post-synaptic rates. *Int. J. Bifurc. Chaos* **1,** 873–890.
53. Segundo J., Diez Martinez O. and Quijano H. (1987) Testing a model of excitatory interaction between pacemakers. *Biol. Cybern.* **55,** 355–365.
54. Segundo J., Stiber M., Altshuler E. and Vibert J.-F. (1993) Transients in the inhibitory driving of neurons and their postsynaptic consequences. *Neuroscience* **62,** 459–480.
55. Segundo J., Stiber M. and Vibert J.-F. (1995) Synaptic coding of spike trains. In *The Handbook of Brain Theory and Neural Networks* (ed. Arbib M.), pp. 953–956. MIT Press, Cambridge, MA.
56. Segundo J., Stiber M., Vibert J.-F. and Hanneton S. (1994) Periodically modulated inhibition and its postsynaptic consequences. II. Influence of pre-synaptic slope, depth, range, noise and of postsynaptic natural discharges. *Neuroscience* **68,** 693–719.
57. Segundo J., Vibert J.-F., Pakdaman K., Stiber M. and Diez Martínez O. (1994) Noise and the neurosciences: a long history, a recent revival and some theory. In *Origins: Brain and Self-Organization* (ed. Pribram K.), pp. 300–332. Lawrence Erlbaum Associates, Hillsdale, NJ.
58. Segundo J., Vibert J.-F. and Stiber M. (1998) Periodically-modulated inhibition and its postsynaptic consequences. III. The heterogeneity of the postsynaptic spike trains, and how control parameters affect it. *Neuroscience* **87,** 15–47.
59. Segundo J., Vibert J.-F., Stiber M. and Hanneton S. (1994) Periodically modulated inhibition and its postsynaptic consequences. I. General features. influence of presynaptic frequency and period. *Neuroscience* **68,** 693–719.
60. Stiber M. (1992) *Dynamics of Synaptic Integration*. Ph.D. thesis, University of California, Los Angeles.
61. Stiber M., Pakdaman K., Vibert J.-F., Boussard E., Segundo J., Nomura T., Sato S. and Doi S. (1997) Complex responses of living neurons to pacemaker inhibition: a comparison of dynamical models. *Biosystems* **40,** 177–188.
62. Stiber M. and Segundo J. (1993) Dynamics of synaptic transfer in living and simulated neurons. In *Proc. ICNN-93*, pp. 75–80. San Francisco, CA.
63. Sugihara G. (1994) Nonlinear forecasting for the classification of natural time series. *Phil. Trans. R. Soc. Lond. A* **348,** 477–495.
64. Sugihara G., Allan W., Sobel D. and Allan K. (1996) Nonlinear control of heart rate variability in human infants. *Proc. natn. Acad. Sci. U.S.A.* **93,** 2608–2613.
65. Sugihara G., Casdagli M., Habjan E., Hess D., Holland G. and Penner R. (1998) Is the atmosphere really chaotic? Nonlinearity in observed barometric pressure records: latitudinal gradients, dominant mechanisms, and improved forecasts. *Nature* (submitted).
66. Sugihara G., Greenfell B. and May R. (1990) Distinguishing error from chaos in ecological time series. *Phil. Trans. R. Soc. Lond. B.* **330,** 235–251.
67. Sugihara G. and May R. (1990) Nonlinear forecasting as a way of distinguishing chaos from measurement error in time series. *Nature* **344,** 734–741.
68. Takahashi N., Hanyu Y., Nusha T., Kubo R. and Matsumoto G. (1990) Global bifurcation structure in periodically stimulated giant axons of squid. *Physica D* **43,** 318–334.
69. Takens F. (1980) Detecting strange attractors in turbulence. In *Dynamical Systems and Turbulence*, Springer Lecture Notes in Mathematics (eds Rand D. and Young L.), Vol. 898, pp. 366–381. Springer, NY.
70. Vibert J.-F., Caille D. and Segundo J. (1981) Respiratory oscillator entrainment by periodic vagal afferents: an experimental test of a model. *Biol. Cybern.* **41,** 119–130.
71. Vibert J.-F., Caille D. and Segundo J. (1985) Examination with a computer at how parameter changes and variabilities influence a model of oscillator entrainment. *Biol. Cybern.* **53,** 1–13.
72. Vibert J.-F., Pakdaman K. and Azmy N. (1994) Inter-neural delay modification synchronizes biologically plausible neural networks. *Neural Networks* **7,** 589–607.
73. Xie M., Pribram K. and King J. (1994) Are neural spike trains deterministically chaotic or stochastic processes? In *Proceedings of the Second Appalachian Conference on Behavioral Neurodynamics* (ed. Pribram K.), pp. 254–267.